



Calhoun: The NPS Institutional Archive
DSpace Repository

Theses and Dissertations

1. Thesis and Dissertation Collection, all items

2012-09

Improving Identification of Area Targets by Integrated Analysis of Hyperspectral Data and Extracted Texture Features

Bangs, Corey F.

Monterey, California. Naval Postgraduate School

<http://hdl.handle.net/10945/17317>

Downloaded from NPS Archive: Calhoun



Calhoun is a project of the Dudley Knox Library at NPS, furthering the precepts and goals of open government and government transparency. All information contained herein has been approved for release by the NPS Public Affairs Officer.

Dudley Knox Library / Naval Postgraduate School
411 Dyer Road / 1 University Circle
Monterey, California USA 93943

<http://www.nps.edu/library>



NAVAL POSTGRADUATE SCHOOL

MONTEREY, CALIFORNIA

THESIS

**IMPROVING IDENTIFICATION OF AREA TARGETS BY
INTEGRATED ANALYSIS OF HYPERSPECTRAL DATA
AND EXTRACTED TEXTURE FEATURES**

by

Corey F. Bangs

September 2012

Thesis Advisor:
Second Reader:

Fred. A. Kruse
Richard C. Olsen

Approved for public release; distribution is unlimited

THIS PAGE INTENTIONALLY LEFT BLANK

REPORT DOCUMENTATION PAGE			Form Approved OMB No. 0704-0188	
Public reporting burden for this collection of information is estimated to average 1 hour per response, including the time for reviewing instruction, searching existing data sources, gathering and maintaining the data needed, and completing and reviewing the collection of information. Send comments regarding this burden estimate or any other aspect of this collection of information, including suggestions for reducing this burden, to Washington headquarters Services, Directorate for Information Operations and Reports, 1215 Jefferson Davis Highway, Suite 1204, Arlington, VA 22202-4302, and to the Office of Management and Budget, Paperwork Reduction Project (0704-0188) Washington DC 20503.				
1. AGENCY USE ONLY (Leave blank)		2. REPORT DATE September 2012	3. REPORT TYPE AND DATES COVERED Master's Thesis	
4. TITLE AND SUBTITLE Improving Identification of Area Targets by Integrated Analysis of Hyperspectral Data and Extracted Texture Features			5. FUNDING NUMBERS	
6. AUTHOR(S) Corey F. Bangs				
7. PERFORMING ORGANIZATION NAME(S) AND ADDRESS(ES) Naval Postgraduate School Monterey, CA 93943-5000			8. PERFORMING ORGANIZATION REPORT NUMBER	
9. SPONSORING /MONITORING AGENCY NAME(S) AND ADDRESS(ES) N/A			10. SPONSORING/MONITORING AGENCY REPORT NUMBER	
11. SUPPLEMENTARY NOTES The views expressed in this thesis are those of the author and do not reflect the official policy or position of the Department of Defense or the U.S. Government. IRB Protocol number ___N/A___.				
12a. DISTRIBUTION / AVAILABILITY STATEMENT Approved for public release; distribution is unlimited			12b. DISTRIBUTION CODE A	
13. ABSTRACT (maximum 200 words) Hyperspectral data were assessed to determine the effect of integrating spectral data and extracted texture features on classification accuracy. Four separate spectral ranges (hundreds of spectral bands total) were used from the VNIR-SWIR portion of the electromagnetic spectrum. Haralick texture features (contrast, entropy, and correlation) were extracted from the average grey level image for each range. A maximum likelihood classifier was trained using a set of ground truth ROIs and applied separately to the spectral data, texture data, and a fused dataset containing both types. Classification accuracy was measured by comparison of results to a separate verification set of ROIs. Analysis indicates that the spectral range used to extract the texture features has a significant effect on the classification accuracy. This result applies to texture-only classifications as well as the classification of integrated spectral and texture data sets. Overall classification improvement for the integrated data sets was near 1%. Individual improvement of the Urban class alone showed approximately 9% accuracy increase from spectral-only classification to integrated spectral and texture classification. This research demonstrates the effectiveness of texture features for more accurate analysis of hyperspectral data and the importance of selecting the correct spectral range used to extract these features.				
14. SUBJECT TERMS Texture, Classification, Hyperspectral, Area targets, Land use classification			15. NUMBER OF PAGES 97	
			16. PRICE CODE	
17. SECURITY CLASSIFICATION OF REPORT Unclassified	18. SECURITY CLASSIFICATION OF THIS PAGE Unclassified	19. SECURITY CLASSIFICATION OF ABSTRACT Unclassified	20. LIMITATION OF ABSTRACT UU	

THIS PAGE INTENTIONALLY LEFT BLANK

Approved for public release; distribution is unlimited

**IMPROVING IDENTIFICATION OF AREA TARGETS BY INTEGRATED
ANALYSIS OF HYPERSPECTRAL DATA AND EXTRACTED TEXTURE
FEATURES**

Corey F. Bangs
Civilian, Department of the Navy
B.S., Keene State College, 2006

Submitted in partial fulfillment of the
requirements for the degree of

MASTER OF SCIENCE IN REMOTE SENSING INTELLIGENCE

from the

**NAVAL POSTGRADUATE SCHOOL
September 2012**

Author: Corey F. Bangs

Approved by: Fred. A. Kruse
Thesis Advisor

Richard C. Olsen
Second Reader

Dan Boger
Chair, Department of Information Science

THIS PAGE INTENTIONALLY LEFT BLANK

ABSTRACT

Hyperspectral data were assessed to determine the effect of integrating spectral data and extracted texture features on classification accuracy. Four separate spectral ranges (hundreds of spectral bands total) were used from the VNIR-SWIR portion of the electromagnetic spectrum. Haralick texture features (contrast, entropy, and correlation) were extracted from the average grey level image for each range. A maximum likelihood classifier was trained using a set of ground truth ROIs and applied separately to the spectral data, texture data, and a fused dataset containing both types. Classification accuracy was measured by comparison of results to a separate verification set of ROIs. Analysis indicates that the spectral range used to extract the texture features has a significant effect on the classification accuracy. This result applies to texture-only classifications as well as the classification of integrated spectral and texture data sets. Overall classification improvement for the integrated data sets was near 1%. Individual improvement of the Urban class alone showed approximately 9% accuracy increase from spectral-only classification to integrated spectral and texture classification. This research demonstrates the effectiveness of texture features for more accurate analysis of hyperspectral data and the importance of selecting the correct spectral range used to extract these features.

THIS PAGE INTENTIONALLY LEFT BLANK

TABLE OF CONTENTS

I.	INTRODUCTION.....	1
II.	BACKGROUND.....	3
A.	PREVIOUS WORK.....	3
1.	Hyperspectral Imaging	3
a.	<i>Spectroscopy</i>	3
b.	<i>Imaging Spectrometry</i>	3
2.	Hyperspectral Analysis	4
a.	<i>General Information</i>	4
b.	<i>Dimensionality Reduction</i>	5
c.	<i>Maximum Likelihood Classification</i>	6
3.	Texture Analysis	6
a.	<i>General Description of Texture</i>	6
b.	<i>Haralick Texture Features</i>	7
c.	<i>Entropy – The Measure of Disorder</i>	8
d.	<i>Optimum Texture Features for Classification</i>	8
e.	<i>Texture Processing Window Size</i>	9
f.	<i>Alternative to Haralick Texture Features</i>	10
4.	Integrated Analysis.....	10
a.	<i>General Information</i>	10
b.	<i>Combining Spectral and Texture</i>	11
B.	AREA OF INVESTIGATION	14
III.	METHODOLOGY.....	17
A.	ATMOSPHERIC CORRECTION.....	17
1.	Purpose	17
2.	Quick Atmospheric Correction (QUAC).....	17
B.	AVIRIS REMOTE SENSING PLATFORM & DATA.....	19
C.	GENERAL PROCEDURE	20
1.	Data Preparation	20
2.	ROI Selection	23
3.	Application of MNF Transform	25
4.	Classification	27
IV.	RESULTS AND ANALYSIS.....	29
A.	SPECTRAL AND TEXTURE ROI AVERAGES	29
1.	Set One: 365–928 nm.....	29
2.	Full Range: 365–2466 nm.....	32
B.	CLASSIFICATION IMAGES	35
1.	Set One: 365–928 nm.....	35
2.	Full Range: 365–2466 nm.....	36
C.	CONFUSION MATRICES	36
1.	Set One: 365–928 nm.....	36
2.	Full Range: 365–2466 nm.....	39
D.	CLASSIFICATION ACCURACY SUMMARY CHARTS.....	40

1.	Spectral-Only Classification Accuracy	40
2.	Texture-Only Classification Accuracy	41
3.	Spectral and Texture Classification Accuracy	41
V.	SUMMARY AND CONCLUSIONS	43
A.	SUMMARY	43
B.	CONCLUSIONS	44
VI.	FUTURE WORK	47
A.	FINER SUBSETS OF THE SPECTRAL RANGE.....	47
B.	HIGHER SPATIAL RESOLUTION IMAGERY	47
C.	OTHER TEXTURE MEASURES	47
APPENDIX	49
A.	SPECTRAL PLOTS	49
1.	Set One: 365–928 nm.....	49
2.	Set Two: 947–1343 nm	49
3.	Set Three: 1432–1801 nm.....	50
4.	Set Four: 1957–2466 nm.....	50
5.	Full Range: 365–2466 nm	51
B.	TEXTURE FEATURE PLOTS	52
1.	Set One: 365–928 nm.....	52
2.	Set Two: 947–1343 nm	53
3.	Set Three: 1432–1801 nm.....	53
4.	Set Four: 1957–2466 nm.....	54
5.	Full Range: 365–2466 nm	54
C.	TEXTURE FEATURE MNF 95% PLOTS	55
1.	Set One: 365–928 nm.....	55
2.	Set Two: 947–1343 nm	56
3.	Set Three: 1432–1801 nm.....	56
4.	Set Four: 1957–2466 nm.....	57
5.	Full Range: 365–2466 nm	57
D.	CLASSIFICATION IMAGES	58
1.	Set One: 365–928 nm.....	58
2.	Set Two: 947–1343 nm	60
3.	Set Three: 1432–1801 nm.....	62
4.	Set Four: 1957–2466 nm.....	64
5.	Full Range: 365–2466 nm.....	66
E.	CONFUSION MATRICES	67
1.	Set One: 365–928 nm.....	67
2.	Set Two: 947–1343 nm	69
3.	Set Three: 1432–1801 nm.....	70
4.	Set Four: 1957–2466 nm.....	71
5.	Full Range: 365–2466 nm.....	73
LIST OF REFERENCES.....		75
INITIAL DISTRIBUTION LIST		81

LIST OF FIGURES

Figure 1.	Hyperspectral imaging concept (From Chai et al., 2000).....	4
Figure 2.	Method of spectral and spatial integration (From Li & Narayanan, 2004).	12
Figure 3.	Spectral spatial integration method (From Rogge et al., 2007).	13
Figure 4.	Full AVIRIS collection flight line # f110928t01p00r08. Blue box shows subset location used for this study.	15
Figure 5.	True color image of the subset study area.	16
Figure 6.	QUAC process flow (From Bernstein et al., 2012).....	18
Figure 7.	Process flow chart.	21
Figure 8.	Texture data sets process flow.	23
Figure 9.	False color IR-R-G composite image of study area (healthy vegetation shown in red).	24
Figure 10.	Study area showing the selected regions of interest (colors detailed in Table 4).	25
Figure 11.	Confusion matrix and Kappa coefficient equation (From Foody, 2002).	27
Figure 12.	Set one: Spectral average for each ROI.....	30
Figure 13.	Set one: Texture average for each ROI. Band definitions in Table 3 on Page 24.	31
Figure 14.	Set one: Texture average 95% MNF for each ROI.	32
Figure 15.	Full range: Spectral average for each ROI.	33
Figure 16.	Full range: Texture average for each ROI.	34
Figure 17.	Full range: Texture average 95% MNF for each ROI.	35
Figure 18.	Set one classification images from left to right: (1) ROIs, (2) spectral-only, (3) texture-only, (4) spectral and texture.	35
Figure 19.	Full range classification images from left to right: (1) ROIs, (2) spectral-only, (3) texture-only, (4) spectral and texture.	36
Figure 20.	Spectral-only classification accuracy summary.	40
Figure 21.	Texture-only classification accuracy summary.	41
Figure 22.	Spectral and texture classification accuracy summary.	42
Figure 23.	Urban classification accuracy summary. Optimal wavelength range set two (947–1343 nm).....	43
Figure 24.	Dirt Path classification accuracy summary. Optimal wavelength range set two (947–1343 nm).....	44
Figure 25.	Full resolution spectral-only classification image set one.	58
Figure 26.	Full resolution texture-only classification image set one.....	59

Figure 27.	Full resolution spectral and texture classification image set one.	59
Figure 28.	Full resolution spectral-only classification image set two.....	60
Figure 29.	Full resolution texture-only classification image set two.	60
Figure 30.	Full resolution spectral and texture classification image set two.	61
Figure 31.	Full resolution spectral-only classification image set three.	62
Figure 32.	Full resolution texture-only classification image set three.....	62
Figure 33.	Full resolution spectral and texture classification image set three.	63
Figure 34.	Full resolution spectral-only classification image set four.	64
Figure 35.	Full resolution texture-only classification image set four.....	64
Figure 36.	Full resolution spectral and texture classification image set four.	65
Figure 37.	Full resolution spectral-only classification image full range.	66
Figure 38.	Full resolution texture-only classification image full range.	66
Figure 39.	Full resolution spectral and texture classification image full range.	67

LIST OF TABLES

Table 1.	AVIRIS specifications.	19
Table 2.	Range and number of bands in each spectral subset.....	20
Table 3.	Texture band descriptions.	22
Table 4.	ROI color descriptions.	24
Table 5.	Contrast texture feature correlation for set one.	26
Table 6.	Spectral-only confusion matrix results for set one.	37
Table 7.	Texture-only confusion matrix results for set one.	38
Table 8.	Spectral and texture confusion matrix results set one.	38
Table 9.	Summary of confusion matrix results for set one.....	39
Table 10.	Summary confusion matrix for full range.	40
Table 11.	Spectral-only confusion matrix set one.....	67
Table 12.	Texture-only confusion matrix set one.....	68
Table 13.	Spectral and texture confusion matrix set one.....	68
Table 14.	Summary of confusion matrix results for set one.....	68
Table 15.	Spectral-only confusion matrix set two.	69
Table 16.	Texture-only confusion matrix set two.	69
Table 17.	Spectral and texture confusion matrix set two.	69
Table 18.	Summary of confusion matrix results for set two.	70
Table 19.	Spectral-only confusion matrix set three.....	70
Table 20.	Texture-only confusion matrix set three.....	70
Table 21.	Spectral and texture confusion matrix set three.	71
Table 22.	Summary of confusion matrix results for set three.....	71
Table 23.	Spectral-only confusion matrix set four.....	71
Table 24.	Texture-only confusion matrix set four.....	72
Table 25.	Spectral and texture confusion matrix set four.	72
Table 26.	Summary of confusion matrix results for set four.	72
Table 27.	Spectral-only confusion matrix full range.....	73
Table 28.	Texture-only confusion matrix full range.....	73
Table 29.	Spectral and texture confusion matrix full range.....	73
Table 30.	Summary of confusion matrix results for full range.....	74

THIS PAGE INTENTIONALLY LEFT BLANK

LIST OF ACRONYMS AND ABBREVIATIONS

AVIRIS	Airborne Visible & Infrared Imaging Spectrometer
B	Blue
CA	California
FWHM	Full Width Half Max
G	Green
GIS	Geographic Information System
GLCM	Gray Level Co-occurrence Matrix
HRV	High Resolution Visible
HSI	Hyperspectral Imaging
Hz	Hertz
IEEE	Institute of Electrical and Electronic Engineers
IMINT	Imagery Intelligence
IR	Infrared
JPL	Jet Propulsion Laboratory
km	Kilometer
LIDAR	Light Detection and Ranging
MLC	Maximum Likelihood Classification
MNF	Minimum Noise Fraction
NASA	National Aeronautics and Space Administration
NIR	Near Infrared
nm	Nanometer
QUAC	Quick Atmospheric Correction
R	Red
RADAR	Radio Detection and Ranging
ROI	Region of Interest
SAR	Synthetic Aperture RADAR
SIPS	Spectral Image-Processing System
SNR	Signal to Noise
SPOT	System for Earth Observation
SWIR	Short Wave Infrared
VIS	Visible
VNIR	Visible and Near Infrared

THIS PAGE INTENTIONALLY LEFT BLANK

I. INTRODUCTION

Many remote sensing platforms collect electro optic data. These systems vary in spectral range and band width as well as spatial extent and resolution. Computer image processing algorithms tend to focus on the spectral character of individual pixels. In the case of hyperspectral data (spatial-spectral data with up to hundreds of spectral bands; Goetz et al., 1985), algorithms may attempt to assign each pixel with a value based on its spectrum and its relationship to other predefined (library) spectra. A classification image is made by grouping pixels with similar values. This is the conventional approach to spectral-only classification.

The process of classifying a single pixel in multispectral and hyperspectral imaging data typically relies solely on the measured spectrum for that pixel, without reference to surrounding pixels. If the target of interest spans an area of several pixels or more, however, there is the potential of using additional information from surrounding pixels in the classification. This information, called texture, is based on the spatial relationship of varying intensity values. The problem with the current method of identification is that even when the target spans many pixels, the texture properties of the target are not being utilized.

Texture extraction is generally accomplished using a gray-level image, however, there are many options regarding the gray level image source. A panchromatic image could be used, which can be advantageous in that it tends to provide the highest spatial resolution of all the types of electro optical collections. Any one of the tens of multispectral bands could be used or one of the hundreds of hyperspectral bands could be used as well. In the case of hyperspectral data, a single band can be used as the gray level image or an average can be taken of more than one spectral band. Additionally any combination of bands could be combined to create a gray scale image.

Texture analysis is important because very valuable information, which is already being collected, can be used to improve the classification accuracy of spectral methods. Substantial previous work combined multispectral data and texture features extracted from co-registered panchromatic data. Olsen et al., 2003 described an application of this approach for the analysis of wetlands areas. Other research used texture to distinguish between spectrally similar tree and lawn classes (Zhang, 2001). In this case, the addition of texture data to the multispectral data showed an average classification improvement of 30% for the tree class compared to conventional spectral-only classification.

The research described here explored the effect of the spectral range used as the source for the gray level image and the dependency of the texture-only classifications on the selected spectral region. The hyperspectral data set was divided up into four spectral subsets. Each of these subsets was converted to a gray level image which represented the mean value over those spectral bands. From these four gray level images, separate sets of texture features were extracted. Classification algorithms were run on the spectral bands, texture bands, and the combined spectral and texture bands. Accuracy of the spectral-only, texture-only, and combined classifications were assessed with respect to pre-defined ground truth classes to determine improvements attributable to the combined analysis and spectral range.

II. BACKGROUND

A. PREVIOUS WORK

1. Hyperspectral Imaging

a. Spectroscopy

Spectroscopy is the investigation of material properties by studying the way matter interacts with electromagnetic radiation. A quantized unit of this radiation is known as a photon. In principle, a target material will either transmit, absorb, or reflect a photon based on its wavelength. Due to the quantum nature of this interaction, a photon of a given wavelength has a probability of transmitting, absorbing, or reflecting upon interacting with a given material. This probability leads to a percentage of the incident energy resulting in some transmission, some absorption and some reflection where the sum total is unity. In a laboratory setting, the full range of the electromagnetic spectrum can be used to probe a material in order to determine its response. A materials response to the full range, or a section of the electromagnetic spectrum can serve as a unique identifier for that material (Vane & Goetz, 1988).

b. Imaging Spectrometry

Also known as hyperspectral imaging (HSI), imaging spectrometry is the collection of the full spectroscopic response over a range of spatial positions, usually using hundreds of spectral bands. This method has proven effective in material identification and mapping based on spectral signatures (Goetz et al., 1985). Figure 1 shows the basic concept of these collection systems.

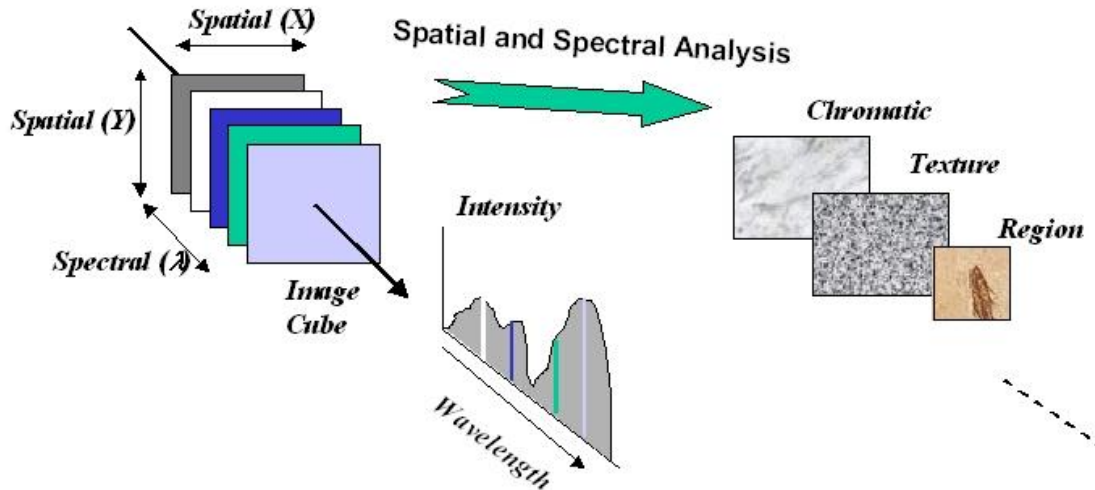


Figure 1. Hyperspectral imaging concept (From Chai et al., 2000).

Hyperspectral imaging has been successfully implemented in a number of airborne and spaceborne systems. The Jet Propulsion Laboratory (JPL) developed a system to take hyperspectral images of the earth. This system is known as the Airborne Visible/Infrared Imaging Spectrometer (AVIRIS) and is an airborne platform which first measured spectral images in 1987 (Green et al., 1998) (Green, 2007). The National Aeronautics and Space Administration (NASA) launched the first space-based sensor covering the visible (VIS) through short wave infrared (SWIR) section of the electromagnetic spectrum. This system, known as Hyperion, is a hyperspectral imager and was launched in 2000 (Pearlman et al., 2003) (Kruse et al., 2003).

2. Hyperspectral Analysis

a. General Information

Hyperspectral analysis is the process by which a target is identified as a known quantity based on its spectral signature. This quantity could come from library spectra or spectra generated using the image itself where a portion of the image has been verified by ground truth. Hyperspectral imagery data provided an analysis challenge when it first began to arrive into the community.

Simply visualizing the data was not easy or intuitive. Work was done to improve this by the creation of algorithms and an interface specifically designed to deal with this type of data (Kruse et al., 1993). Once the data could be worked with in an efficient way, the next step was to process the data. There are many different ways that targets can be matched. These include approaches such as: binary encoding, minimum distance, and maximum likelihood. A survey of many of the most widely used methods has been compiled (Franklin & Wulder, 2002). So far each method has been shown to have its strengths and its weaknesses. Therefore, the method used must be considered based the goals of each endeavor (Franklin & Wulder, 2002). Some methods designed for analysis of multispectral data have been shown to be ineffective when dealing with the higher dimensionality of hyperspectral imaging data. A comparison of classification methods applied to hyperspectral imaging data is shown in Cloutis, 1996.

b. Dimensionality Reduction

One approach used often in the analysis of hyperspectral imagery is to start by reducing the dimensionality of the data set. This can be done by a principal components transform, which can reduce hundreds of bands of spectral information to tens, while preserving the vast amount of information from the original data set. The purpose of this is to get at the intrinsic dimensionality of the data set. This will avoid redundancy caused by highly correlated spectral bands (Harsanyi & Chang, 1994). An extension of this is to consider the signal to noise ratio (SNR) during the transform and thus deemphasize the noise contribution; this is known as a minimum noise fraction (MNF) approach (Green et al., 1988) (Boardman & Kruse, 2011). If the classification effort is performed with library spectra, then the transforms can be modified to specifically reject all other signals from the data. Then an optimal classification can be performed on the remaining data. This approach maximizes the ability to classify while minimizing the amount of data to process (Harsanyi & Chang, 1994). The maximum likelihood method of hyperspectral classification is used so often that work has been put into

optimizing it to process large data sets such as those obtained by the use of the AVIRIS system (Roger, 1996). The maximum likelihood classification method has been extended to incorporate prior probabilities when training sets yield this information (Strahler, 1980). Varying atmospheric and illumination conditions can make matching target spectra with library spectra difficult. Work has been done, however in the area of automating identification under these unknown conditions (Healey & Slater, 1999).

c. Maximum Likelihood Classification

The maximum likelihood classification method is a statistically based classification method. Each pixel that is processed is assigned to the class that it has the highest probability of being a member. To do this statistically an assumption must be made, which is that the statistical distribution of each class is normal. This method is computationally expensive and because of this has not always been utilized even though it has been around since around 1912 (Hald, 1999). It has been confirmed that the maximum likelihood classification method does assign pixels to the class they most likely belong when hyperspectral imagery data is used (Cloutis, 1996). Work continues to improve the use of maximum likelihood classification on hyperspectral imagery data sets. With large pixel sizes the training set can be too small to generalize the classification. A method has been presented to find near neighbors that can be included in the training set if they will indeed improve the class statistics (Richards & Jia, 2008).

3. Texture Analysis

a. General Description of Texture

Texture is the connection between pixel positions and their intensity values. This is distinct from tone, which is the statistical relationship between a pixel's value and all other pixel values in an image regardless of their position. Both of these are important properties of an image and can be used to process data. Texture has been used to process imagery for a range of disciplines. For

example the field of medical research has used texture to automatically detect heart disease by computer processing x-ray images (Sutton & Hall, 1972). Spectrally similar vegetation classes have been successfully separated by the use of texture (Zhang, 2001). Early work in the recognition of patterns, upon which texture analysis is built, dates back to work done with conditional joint probability densities where the image pixels are processed as a vector (Sebestyen, 1962). General image processing that performs calculations based on the spatial relationship of pixel values and thus the very basis of texture analysis has long been studied (Andrews et al., 1972). Finally, an overview of early work on feature extraction and pattern recognition is noted (Levine, 1969).

b. Haralick Texture Features

The pioneering work of computer based extraction of textural features was published by Haralick in 1973. He described a set of algorithms to process black and white images in such a way as to produce texture features. This work focuses on the grey level spatial dependence relationship using a Grey Level Co-occurrence Matrix (GLCM). From this GLCM the quantities known as texture features are extracted. The textures studied in his landmark paper were: angular second moment, contrast, correlation, sum of squares, variance, inverse difference moment, sum average, sum variance, sum entropy, entropy, difference variance, difference entropy, information measures of correlation, and maximal correlation coefficient. Some success was shown classifying imagery using just these texture features (Haralick et al., 1973). More recent work has been done to compare the Haralick texture features with other methods. Gabor texture filters were found to be outperformed by other methods and there was no evidence they should be preferred. Wavelet transform decomposition was shown to generally not be superior to other decompositions. The final result is that there was not a clearly preferred method and thus no clear alternative to the Haralick texture feature method (Randen & Husoy, 1999).

c. Entropy – The Measure of Disorder

One of the measures of texture put forth by Haralick is entropy, which is a measure of randomness. This quantity first arose in the context of communication theory and was applied to place a limit on the optimal lossless compression for a given set of data (Shannon, 1997). Target classes can vary by randomness, crops will have low randomness due to their uniform rows. A natural forest will exhibit high randomness as a result of growth cycles. In the context of remote sensing this property has the ability to measure texture in a unique and meaningful way that can be combined with other independent measures of surface variation (Shannon, 1997). The Shannon entropy texture feature has successfully been used to measure the compactness of an urban area. A study was done to specifically measure the urban growth and entropy was used as an indicator. The area studied by Bhatta was Kolkata, West Bengal, India. Landsat data were used for the study (1975, 1990, and 2000) as well as data from the Indian multispectral asset Resourcesat 1 (2005). The spectral range used for the study were VIS-NIR and for Landsat TM/ETM+ the SWIR bands were also included. Validation was done using census data to confirm the method was effective before using it to make predictions about the future (Bhatta, 2009).

d. Optimum Texture Features for Classification

There is good reason to wonder which of the texture measures outlined by Haralick should be used, as many of them are directly correlated. Another good question is how many grey levels should be used in the calculation of these texture features. The effect of varying the grey level quantization used to calculate texture features was one topic of this investigation. In the research done by Clausi, 2002 the ability of texture for classification was studied. It was shown, that for some texture features, increasing grey levels can lead to a decrease in the classification accuracy. It was also shown, for the remaining Haralick texture features, that accuracy remained the same for the range of

quantization levels studied. Clause's work has also shown that the most effective classification is achieved with only three texture features, namely: contrast, entropy, and correlation. These three texture features out performed all other texture set combinations and did so with a relatively low quantization level. One benefit to this particular set of texture features is that they are largely independent of each other. The work by Clausi has put bounds on the preferred quantization level between 24 and 64, with levels lower than 24 producing unreliable results and levels higher than 64 failing to improve the classification accuracy (Clausi, 2002). Performance evaluation has been done on the Haralick texture features confirming that contrast, entropy, and correlation are among the most useful features to use for classification (Ohanian, 1992). Some work has been done on complex terrain in which the addition of only the texture feature entropy was sufficient to improve the classification results compared to spectral data only (Franklin & Peddle, 1989).

e. *Texture Processing Window Size*

The next question to consider is the optimum size of the texture window to use for calculating the texture features. This window defines the number of surrounding pixels that are used to create the GLCM. A 3x3 window would only include the 8 pixels immediately adjacent to the pixel being processed. A 5x5 window would include the 8 pixels from the 3x3 window in addition to the 16 pixel immediately adjacent to those 8 pixels. Combining texture features calculated from a range of window sizes has been shown to increase the classification accuracy of forest tree types (Coburn & Roberts, 2004). In this work the term multi-scale refers to the size of the moving processing window used to calculate the texture features. The greatest success of the study showed that a combination of texture features from different window sizes produced better results than any individual window size. The range of window sizes used to determine this were between 3x3 and 11x11. This paper supports the idea that the texture that exists in remotely sensed images is fundamentally multi-dimensional (Coburn & Roberts, 2004). Land use classification work done using

SPOT HRV data supports the use of window sizes including 3x3, 5x5, and 7x7 (Gong et al., 1992). In this study, the larger sizes were omitted because of unsatisfactory preliminary results. It stands to reason that including larger windows is harmless if a dimensionality reduction step is performed before the classification step.

f. Alternative to Haralick Texture Features

An alternative concept for quantifying texture is the texture spectrum using texture units (He & Wang, 1990). A texture unit, defined by He and Wang, is a measure of each pixel's relationship to the eight surrounding pixels. It is a one by eight vector that contains a zero (0) if that neighbor's value is less than the given pixel. The vector contains a one if the neighbor is equal to it and a two if it is greater than. This leads to a total number of possible texture units of 6561. In the method outlined, this is calculated for an area of an image and the results are fashioned into a histogram. This becomes the texture spectrum that can be used as a measure of the texture for a given area and success was achieved in using this as a basis for classification. In the experiments described, the accuracy rate is 97.5% for a mixed texture image, and 99.6% for an image with homogeneous texture (He & Wang, 1990).

4. Integrated Analysis

a. General Information

Integrated analysis is the process that allows multiple types of information to be used together, for a shared purpose, in the most successful way possible. Hyperspectral data can be fused with LIDAR data to perform classification of forest types (Dalponte et al., 2008) or to estimate tree stem diameters (Dalponte et al., 2009). Data fusion can also result in other benefits, like enhanced resolution of hyperspectral imagery data sets (Mianji et al., 2009). With the realization that sometimes, preferred datasets are those that were collected at the same time and from the same view angle, a team set out to do a

coincident collection. A collection of multispectral data and high resolution color imagery data was successfully completed in 2001. These multiple collections were combined to produce a coincident data set that can easily be used for further analysis and processing (Mirzaoff et al., 2002). Another method for the fusion of hyperspectral and high spatial resolution data is to extract spatial information from the high spatial resolution data and use it to modify the hyperspectral data at its original spatial resolution (Niemann et al., 1998). The fusion of hyperspectral and multispectral data sets has been explored by means of different algorithms with a principle component transform being the preferred method. This yielded an image with the spatial resolution of the multispectral data and the spectral resolution of the hyperspectral data (Pande et al., 2009). SAR data and electro-optical data have been successfully fused with the use of support vector machines, which in the case studied out performed, among others, the maximum likelihood classification method (Waske & Benediktsson, 2007). Early work done using aerial photography, multispectral, and thermal imaging data that had been collected at optimal times throughout the year, relative to the information type desired, and were integrated to map inland wetlands (Jensen et al., 1986).

b. Combining Spectral and Texture

There is significant previous research on combining spectral data and texture data to perform supervised classification (Li & Narayanan, 2004). A diagram of the system architecture used by Li is shown in Figure 2. In the approach by Li texture features are extracted from images along with land use classifications. These are combined with a segmentation algorithm and stored in a data base for future query and retrieval.

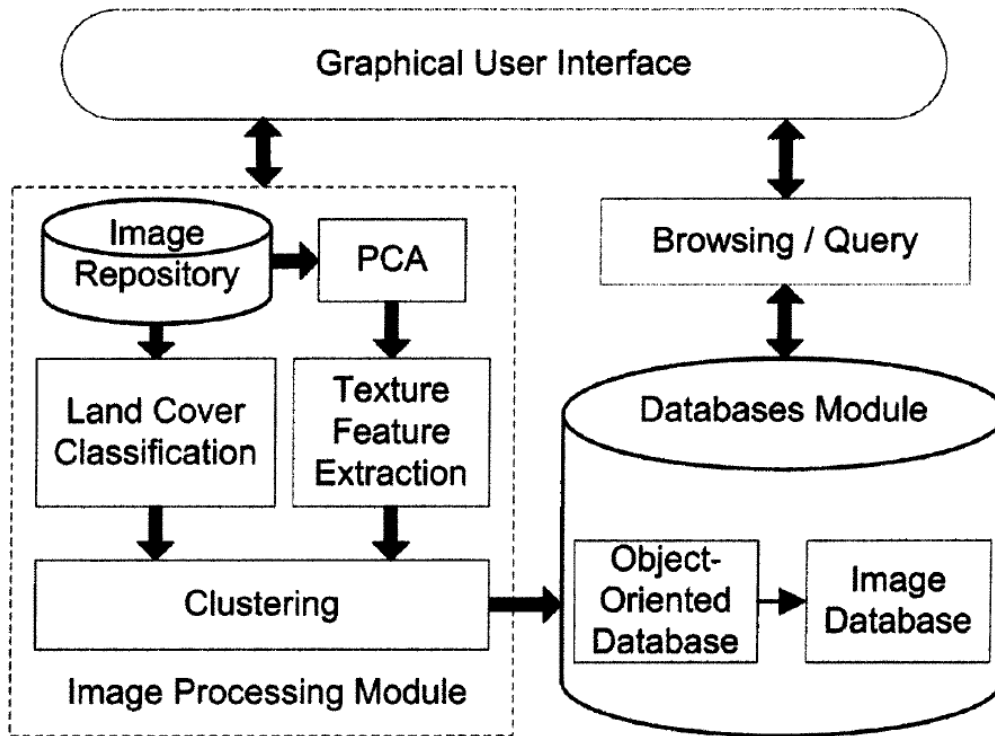


Figure 2. Method of spectral and spatial integration (From Li & Narayanan, 2004).

A method, by Rogge et al. (2007) of endmember extraction based on spatial proximity is an example of combining spectral and spatial information and a diagram is shown in Figure 3. In the work by Rogge pixel spectra were grouped together based on their position to improve endmember selection.

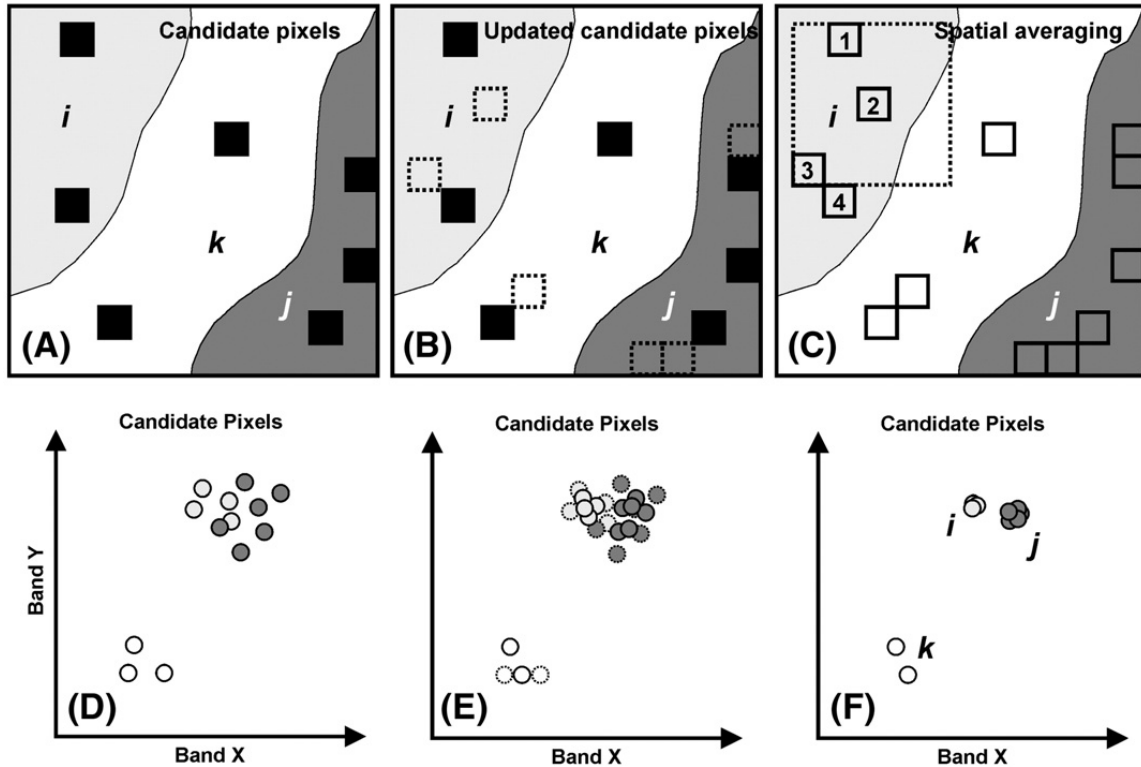


Figure 3. Spectral spatial integration method (From Rogge et al., 2007).

Previous research was also done on image segmentation in the areas of hedges (Lennon et al., 2000) and forests (Ryherd & Woodcock, 1996). Texture has also been used to create optimal composite images, from multiple hyperspectral data sets, to be visually interpreted by a human (Wilson et al., 1997). An example of spectral and texture fusion focused on the classification of wetlands in the Elkhorn Slough on the coast of California (Olsen et al., 2003). The IKONOS satellite sensor was used, which has four spectral bands (4 m resolution) and one panchromatic band (1 m resolution). The panchromatic band was used to extract four virtual texture bands; two for variance and two for correlation. These were combined with the four spectral bands to create an eight band data set. The combined data set was trained using ground truth ROIs and classified using, among others, the maximum likelihood and minimum distance classifiers. At 4 m resolution the accuracy for the spectral-only data set was ~50% while the addition of the texture bands increased this to ~55%. The

minimum distance results for spectral-only were ~27% and adding the texture bands reduced the accuracy to ~9% (Olsen et al., 2003). Other work to classify land use types was done to study the amount of remaining vegetation as an urban area was built up over time. Improvement with the addition of the spatial components was shown for some classes and not for others (Segl et al., 2003). The method of integration that is most relevant to the work done in this research is the combination of spectral and texture bands used by Olsen et al. (2003). This method allows for the use of supervised classification and the comparison of spectral-only, texture-only and combined spectral and texture data sets.

B. AREA OF INVESTIGATION

The data used for this study were AVIRIS data collected over Salinas, CA, and surrounding areas. The collection was done on the 9th of September 2011. Collection began at 8:24pm and concluded at 8:36pm. The instrument was flown at an altitude of 3km with a ground speed of 122km/hr. The resulting resolution is approximately 2.7 m per pixel and the image is 978 x 9643 pixels in size, which can be seen in Figure 4. The coordinates for the center of the subset study area are (+36.709870, -121.664468) and this area is shown in Figure 5. The ground track vector for the flight path started from the north-west and proceeded to the south-east. Some significant regions captured in this collection include Moss Landing, Castroville, and Rt. 101. This area has been studied previously using high-resolution panchromatic imagery to extract texture features (Humphrey, 2003).

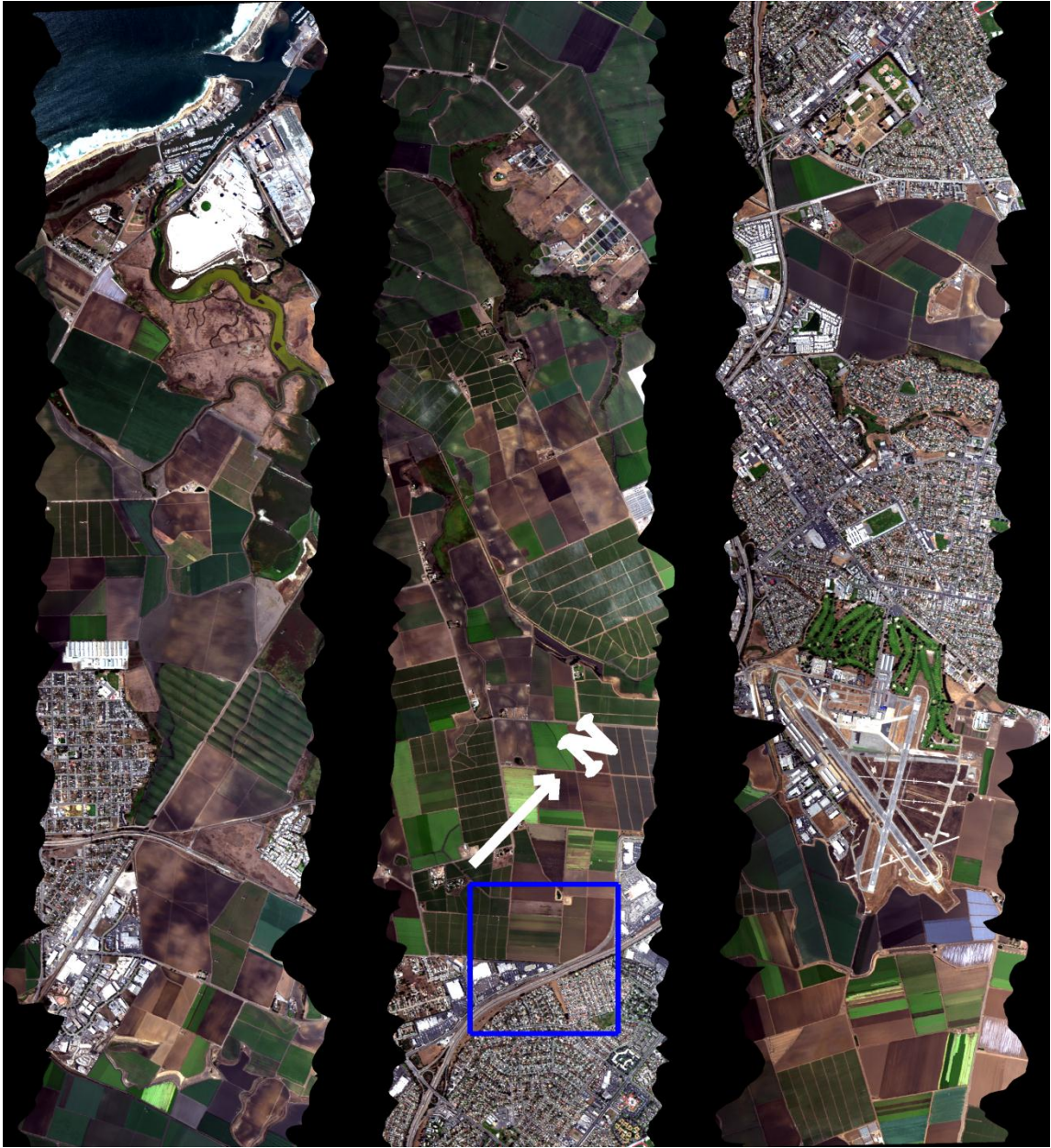


Figure 4. Full AVIRIS collection flight line # f110928t01p00r08. Blue box shows subset location used for this study.



Figure 5. True color image of the subset study area.

The subset study area contains a variety of ground cover types including (1) pavement that can be found on the major highway, parking lots, and mixed in with residential housing; (2) urban mixtures of houses, yards, trees, cars, and dirt; (3) green healthy fields and dry vegetation and mixtures; and (4) dirt paths found between the fields used for agricultural access. These ground cover types can be hard to distinguish using spectral classification only. The dry vegetation and dirt path class for example are nearly identical from a spectral perspective.

III. METHODOLOGY

A. ATMOSPHERIC CORRECTION

1. Purpose

Due to the wavelength dependent nature of atmospheric absorption, radiation incident on the sensor at altitude is not equal to the radiation leaving the target surface on the ground. This means that some form of compensation is required to convert sensor measurements into the spectral reflectance of the target material. After this conversion is made, further processing can take place such as classification using known library spectra, which will now match with the recorded data (Bernstein et al., 2008).

2. Quick Atmospheric Correction (QUAC)

Atmospheric correction for this study was performed using the process known as QUAC. This method has been around for many years and is widely available in the remote sensing community (Bernstein et al., 2004; 2005). The goal is to convert the upwelling radiance recorded at the sensor into apparent reflectance at the target surface. The QUAC algorithm makes a key assumption, which holds for most scenes. That is that the scene contains 10 or more diverse endmembers and that their average reflectance spectrum is constant from scene to scene. This is taken to be a universal reference spectrum, which has been shown empirically (Bernstein et al., 2012). Figure 6 shows the process flow for the algorithm. After the first two setup steps the offset value is obtained by selecting the lowest value in each band. Next, all pixel spectra are divided by the solar blackbody curve as a way to normalize the data set before endmembers are selected. These endmembers are computed with the chosen library endmembers and a gain curve is calculated.

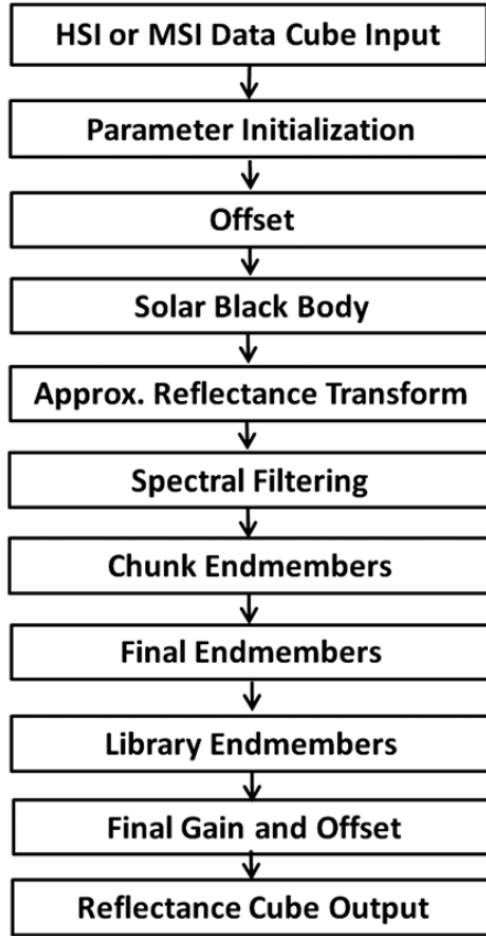


Figure 6. QUAC process flow (From Bernstein et al., 2012).

Equations 1 & 2 are the gain and offset used in the QUAC algorithm. (Bernstein et al., 2012) The numerator of the gain equation is the average of the endmember spectra derived from linear combinations of library spectra. The denominator in the gain equation is the average of the endmembers retrieved from the in-scene pixel spectra. The offset equation yields a curve of minimum values from each spectral band.

$$Gain = \frac{\langle \rho_{end} \rangle_{lib}}{\langle (L_{obs} - C \rho_{ave})_{end} \rangle} \quad (1)$$

$$Offset = \min(pixel_value_for_each_band) \quad (2)$$

B. AVIRIS REMOTE SENSING PLATFORM & DATA

The AVIRIS sensor is a hyperspectral imaging (HSI) system also known as an imaging spectrometer. First measuring spectral images in 1987 AVIRIS, collects upwelling radiance from the solar reflected spectrum from approximately 400–2500 nm. Across this spectrum are 224 bands spaced approximately 10 nm apart with an average band width of 10 nm at FWHM (Green et al., 1998). The AVIRIS specifications are detailed in Table 1. The AVIRIS system can be hosted on several different airframes and flown at different altitudes. The data used for this study were collected using the Twin Otter airframe. At the time of collection the aircraft’s altitude was 3 km and its speed over the ground was 122 km/hr. This resulted in a data set with a ground sample distance of approximately 2.7 m.

Description	Value	Units
Scan Rate	12	Hz
Detectors	224	#
Digitization	12	Bits
Data Rate	20.4	Mbits/sec
Spectrum Rate	7300	Spectra/sec
Wavelength Range	400–2500	nm
Sample Spacing	10	nm
Spectral Response	10	nm
Calibration Accuracy	1	nm
Signal-to-Noise	100:1	Ratio
Field of View	30	Degrees
IFOV	1	mrad
Flight Line Length	800	km

Table 1. AVIRIS specifications.

C. GENERAL PROCEDURE

1. Data Preparation

Once the data were corrected to apparent reflectance using QUAC, the data were spectrally subset into four sets. Spectral band groups were selected to remove the water absorption regions near 1400 and 1900 nm and any noise recognized in the data. This is shown in Table 2.

	# of bands	# removed	Min (nm)	Max (nm)
Set one	61	1	365	928
Set two	44	8	947	1343
Set three	38	17	1432	1801
Set four	52	3	1957	2466
Total	224	29	365	2466

Table 2. Range and number of bands in each spectral subset.

An average image was taken of the bands in each set. For example the gray level image for set one was taken from 61 bands (365–928 nm). These gray scale images were used as the inputs for the texture extraction processes. The texture features extracted were: contrast, entropy, and correlation (Haralick et al., 1973). These have been shown to be optimal, and as a group, they perform better than any single texture measure and better than any other set of traditional Haralick texture features (Clausi, 2002).

The window size used to extract these texture features was varied from 3x3 to 11x11 to capture unique features at different scales. For each window size, all three texture features were extracted. This results in a 15 dimensional texture feature vector, which is detailed in Table 3. After a dimensionality reduction, this data set was used independently to classify area targets as well as being merged with the spectral subset data cube. This vector was rescaled to blend in with the reflectance data during classification. Because the maximum likelihood method was used, any extreme difference in amplitude could bias the

results, therefore a scale factor of x200 was chosen to bring the maximum values of the texture vector up to the maximum values of the spectral data. Rescaling the data minimizes any unintended influence due to this effect. A flow diagram from original data to classification is shown in Figure 7.

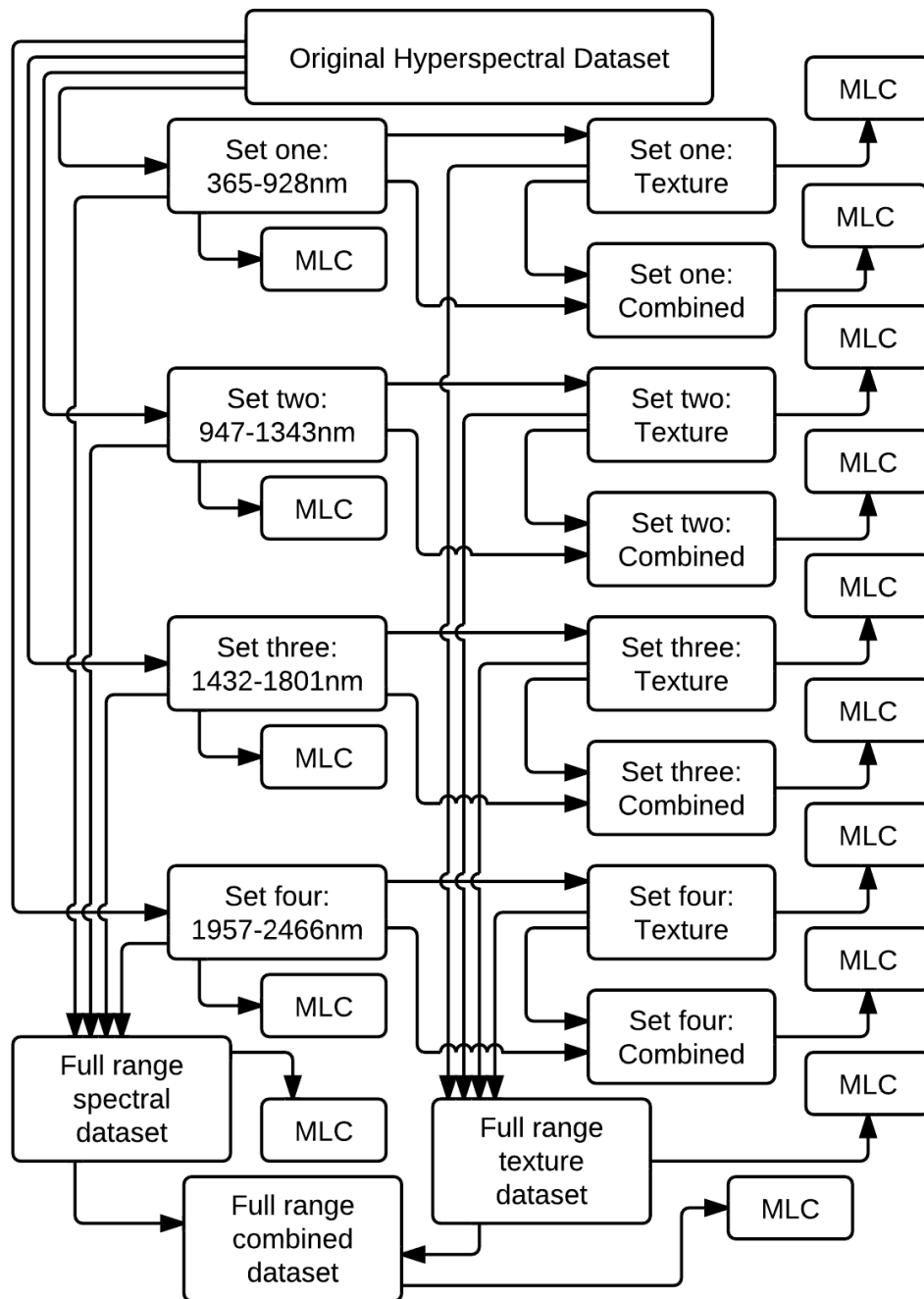


Figure 7. Process flow chart.

Band #	Texture Feature	Window Size
01	Contrast	03x03
02	Entropy	03x03
03	Correlation	03x03
04	Contrast	05x05
05	Entropy	05x05
06	Correlation	05x05
07	Contrast	07x07
08	Entropy	07x07
09	Correlation	07x07
10	Contrast	09x09
11	Entropy	09x09
12	Correlation	09x09
13	Contrast	11x11
14	Entropy	11x11
15	Correlation	11x11

Table 3. Texture band descriptions.

Shown in Figure 8 is the process flow from the original AVIRIS data to final texture data sets. These are the data sets that get classified on their own, combined with spectral data, and finally get combined with all the texture data sets and all the spectral data sets for the full range analysis.

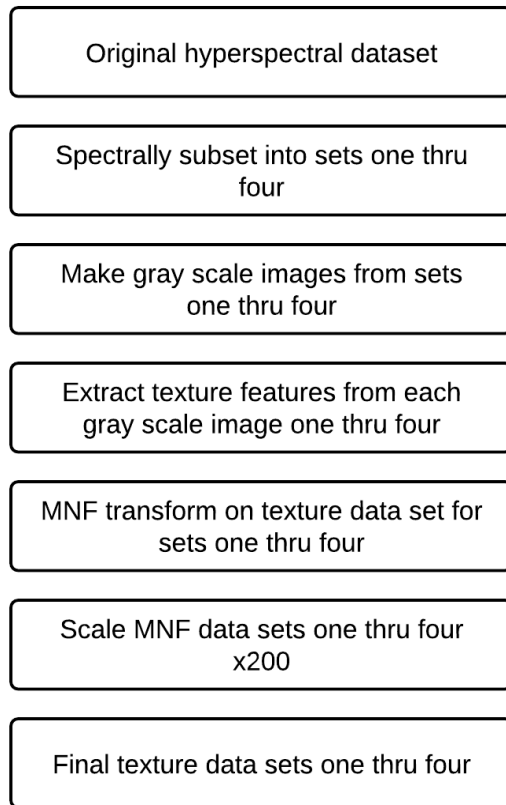


Figure 8. Texture data sets process flow.

2. ROI Selection

Classification of the AVIRIS data were performed using statistical measures rather than by using library spectra. Therefore, training classes were defined by selecting ROIs based on ground truth inferences from Google Earth as well as the study area data. R-G-B true color composites were used to select paved roads and urban areas. A false color IR-R-G composite shown in Figure 9 was used to distinguish dry and healthy vegetation (healthy vegetation appears red). To check the accuracy of these classification methods separate ROIs were selected to be used in the post classification confusion matrices. The ROIs shown in Figure 10 and detailed in Table 4 are all two-tone colors indicating the separate ROIs that were used for training and verification. Each class was initially selected as a single ROI for a total of five separate ROIs. Next, half the number of pixels from each class were chosen randomly and became the training

set (total of five training ROIs). Then the remaining pixels from each class became the verification set (total of five verification ROIs). In this way, the full extent of the selected classes are used. ROIs are evenly distributed into training and verification data sets.



Figure 9. False color IR-R-G composite image of study area (healthy vegetation shown in red).

Class	Color	Used for
Dry Veg	Red	Training
Dry Veg	Dark Red	Verification
Healthy Veg	Green	Training
Healthy Veg	Dark Green	Verification
Urban	Cyan	Training
Urban	Dark Cyan	Verification
Dirt Path	Blue	Training
Dirt Path	Dark Blue	Verification
Pavement	Maroon	Training
Pavement	Dark Maroon	Verification

Table 4. ROI color descriptions.

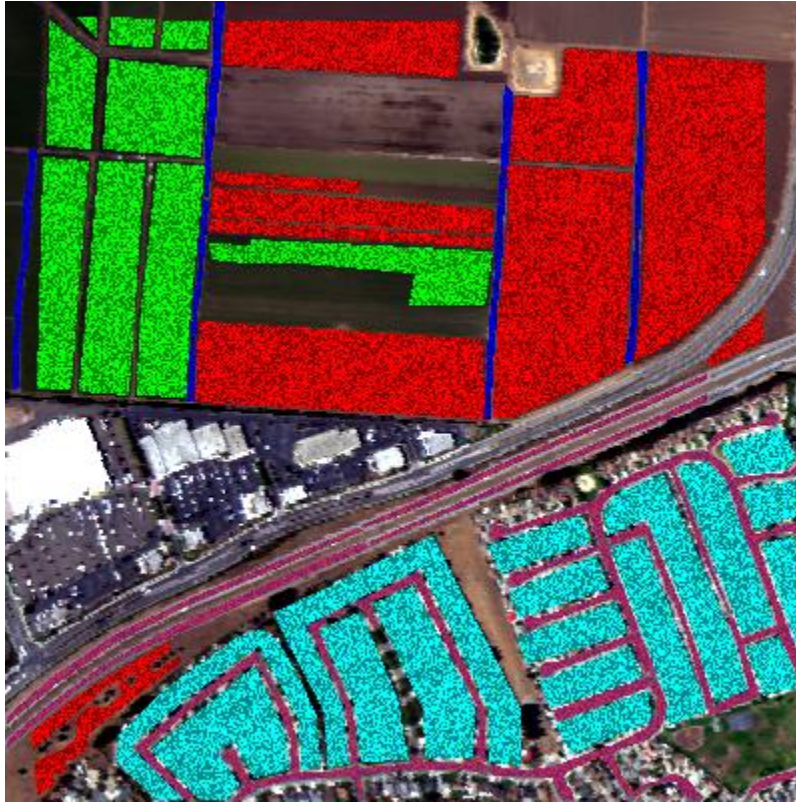


Figure 10. Study area showing the selected regions of interest (colors detailed in Table 4).

3. Application of MNF Transform

At this point we have eight groups of data, the four spectral subsets and the extracted texture data sets that go with each spectrally subset region. Each of these texture subsets underwent a dimensionality reduction before moving on to the next process of classification and then accuracy verification. The dimensionality reduction is necessary for the extracted texture sets because there are some very clear correlations in the data that will lead to less accurate classification. This is likely due, in part, to the added noise from each correlated band whereby these additional bands do not add new information but do add more noise to the data set. This can be understood by considering the three extracted texture features that get repeated with an increasing window size. The texture measure correlation for example will increase as the window size increases in a uniform area such as a field. As a result, it is clear that many of

those data points will be correlated. The MNF transform is able to order the data by descending signal to noise ratio for each of the dimensions (Green et al., 1988; Boardman & Kruse, 2011). Then the dimensions with the least signal to noise can be removed. For this research, the 15 dimension texture data sets were reduced to six dimensions that accounted for 95% of the original information in that data set. In addition to removing noise from the data sets, the extensive correlation found in the data set was removed, which is expressed by the removal of nine bands of the texture data. As an example, the correlation of the contrast texture features are shown in Table 5. The spectral data were not dimensionally reduced. While there is perhaps something to be gained by this, the purpose of this research was to demonstrate an improvement over traditional spectral-only classification methods. Performing a MNF on the spectral data would only confuse the matter at hand.

Correlation	Band 01	Band 04	Band 07	Band 10	Band 13
Band 01	1.000	0.878	0.785	0.705	0.645
Band 04	0.878	1.000	0.933	0.863	0.796
Band 07	0.785	0.933	1.000	0.954	0.899
Band 10	0.705	0.863	0.954	1.000	0.964
Band 13	0.645	0.796	0.899	0.964	1.000

Table 5. Contrast texture feature correlation for set one.

A scale factor is required so the MNF texture data match values with the spectral data. This scale factor was determined by comparing the minimum and maximum values of the spectral and MNF texture data. The entire subset image was used, not just the ROIs selected for training and verification. This was done so the scale factor would be less specific to the ROIs used. The scale factor of 200, calculated in this way, will be more representative of the appropriate scale relationship between the spectral data to the MNF texture data. Because of this, the spectral and MNF texture data ranges of the ROIs shown do not match exactly.

4. Classification

To investigate the improvement of identification each data set was processed using the supervised classification method known as maximum likelihood, previously described. Each data set was used to classify the study area using the training ROIs as input to the classification algorithm. The resulting classification image was measured for accuracy by comparing it to the verification ROIs. The summary of this is captured in a confusion matrix. A confusion matrix is a way of displaying the results of two classification images when one is considered to be ground truth. The second image is rated by what percent of pixels agree with the ground truth image. This is typically broken up class by class as well as providing an overall accuracy percentage measurement. In addition to this a separate overall measurement is produced which takes into account the size of each class and weights the contribution to this measurement, known as the kappa coefficient, by the proportion of each class compared to the total classification area. In this way, small classes that do very well carry less weight than large classes that do poorly, which could bias the results. The equations for the percent correct and kappa coefficient measurements are shown in Figure 11.

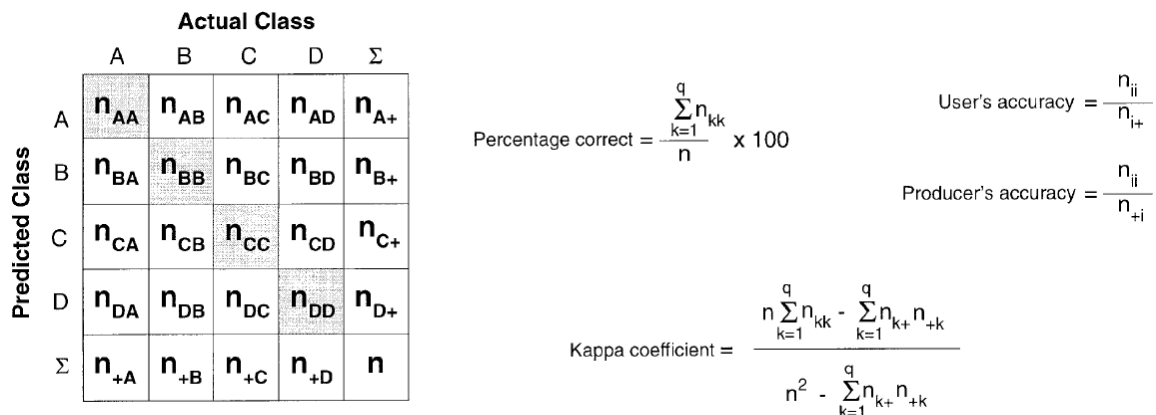


Figure 11. Confusion matrix and Kappa coefficient equation (From Foody, 2002).

Classifications were performed for the spectral-only, texture-only, as well as combined spectral and texture data sets. This included individual processing for each of the four spectral subset regions and the full spectral and texture data sets.

IV. RESULTS AND ANALYSIS

A. SPECTRAL AND TEXTURE ROI AVERAGES

The following are the results for the first spectral set and the full spectral range. The remaining results for spectral sets one thru four are detailed in the Appendix. Each spectral subsets results consist of the following items for each ROI: average spectra, average texture features, average texture features after MNF transform. Classification images include: spectral-only, texture-only, and combined spectral and texture. Confusion matrices include: spectral-only, texture-only, and combined spectral and texture. Also included are the combined results for comparison, which are spectral, texture, and combined spectral and texture confusion matrix summaries for each spectral range one thru four and the full range. Lastly are classification accuracy summaries for spectral-only, texture-only, and spectral and texture data sets.

1. Set One: 365–928 nm

Shown in Figure 12 are the average spectra for each of the ROIs. This data is the scaled reflectance as it is output from QUAC, the data range is approximately +100 to +4000 (1 to 40% reflectance). In this spectral range we see an expected profile for healthy vegetation with a peak near 550 nm, an absorption feature near 675 nm, and a large peak near (IR plateau) 900 nm. The dry vegetation is characterized by the lack of an absorption feature near 675 nm and the lack of a large peak near 900 nm. Pavement shows a characteristic (dark) profile having no sharp features and a gradual increase throughout this spectral range. The Dirt Path is lacking the absorption feature near 675 nm and increases from low to high wavelengths. The Urban class is similar to the Dirt Path profile but with less of an increase from low to high wavelengths.

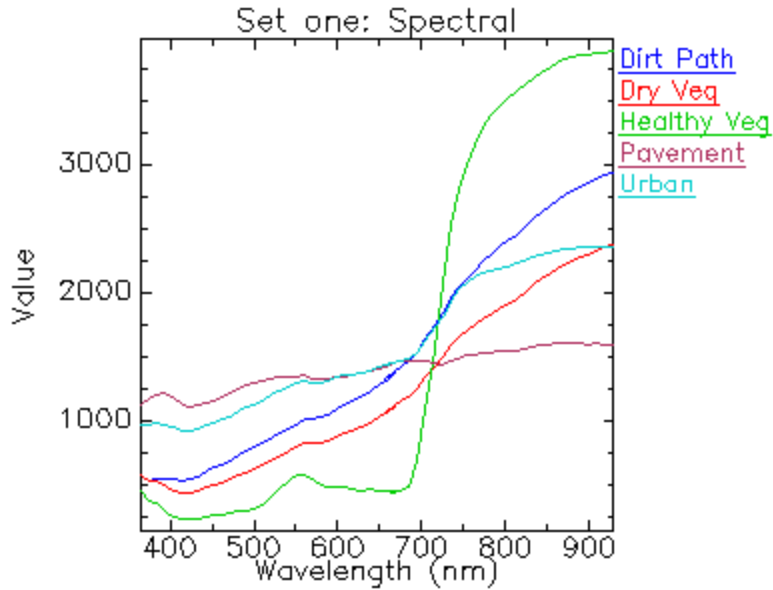


Figure 12. Set one: Spectral average for each ROI.

A plot of the texture features shown in Figure 13 is less intuitive than the spectral signatures are in describing their relationship to a particular material. The band numbers for these texture feature plots are defined in Table 3. This is the point of the study, that is, to draw on additional unique information from the area targets in question. This information is not accessible from the individual pixel spectra, which is what points the research towards extracting texture features. For example if any of these ROI materials were carefully arranged such that they were smoothly and evenly distributed over a large area they would yield a large correlation value with small entropy and contrast values. The goal of this study is to consider how these materials are normally found and what their arrangement typically is for the scene in question. We also can show that these target classes are typically arranged in such a way as to provide valuable texture feature identifiers. Shown in Table 3 bands 3, 6, 9, 12, and 15 are correlation texture features. So areas where one pixel's value can be used to predict the values of neighboring pixels would have a high measure of correlation. This can be seen in the dry vegetation class indicating that this class has high degree of correlation. The data shown below have not been scaled, these are the results

from the texture extraction process, the range is approximately -10 to +450. This raw texture data was not used directly for classification, it is shown here to illustrate the texture extraction results. These data were used as input to the MNF transform.

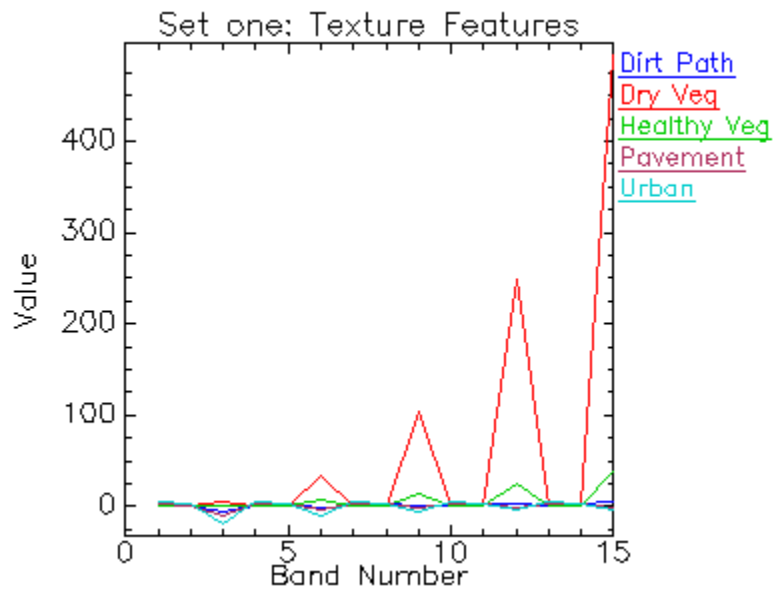


Figure 13. Set one: Texture average for each ROI. Band definitions in Table 3 on Page 22.

We have seen that these texture bands can be correlated. The best way of dealing with this type of data is to perform a MNF transform. In this case, 95% of the information was retained before proceeding to the next processing step. These new bands are shown in Figure 14 and represent the information from the extracted texture feature bands but have been decorrelated and much of the noise has been removed so they don't look like the raw texture feature bands. The MNF texture data shown have been scaled by a factor of 200 to match the spectral data sets. The data range is approximately -2500 to +3000.

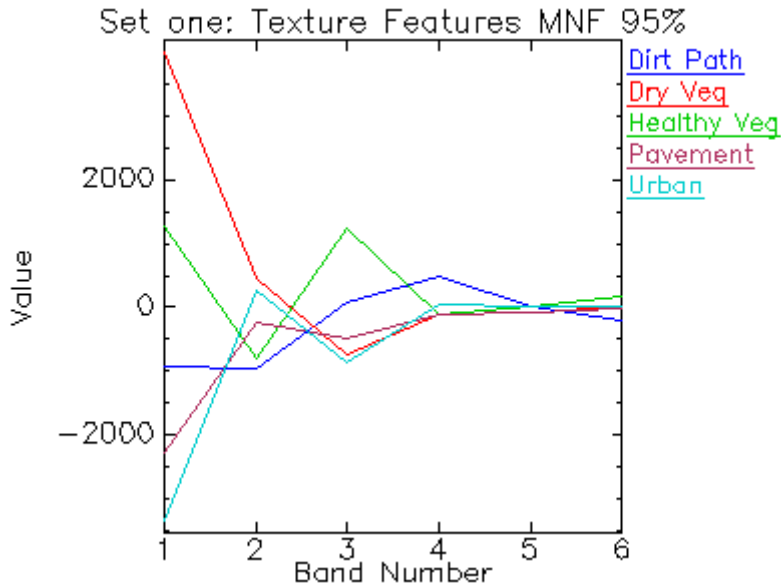


Figure 14. Set one: Texture average 95% MNF for each ROI.

2. Full Range: 365–2466 nm

These full range results follow from the first subset results. Shown in Figure 15 the ROIs discussed earlier display their reflectance profile across the full spectral range of the AVIRIS system. This data is the scaled reflectance as it is output from QUAC, the data range is approximately +100 to +4500 (1 to 45% reflectance). The two classes Dirt Path and Dry Veg show an absorption feature at 2200 nm, which indicates the presence of a mineral. In the case of a Dirt Path one expects to see the sign of minerals. For Dry Veg the sign of minerals may cause concern of incorrect ground truth. It is noted, however, that with Dry Veg there is considerably more penetration thru to the ground below which is made up of, among other things, minerals. Thus, in fact, the dry vegetation class is likely a mixture of dry vegetation and “dirt” spectral signatures.

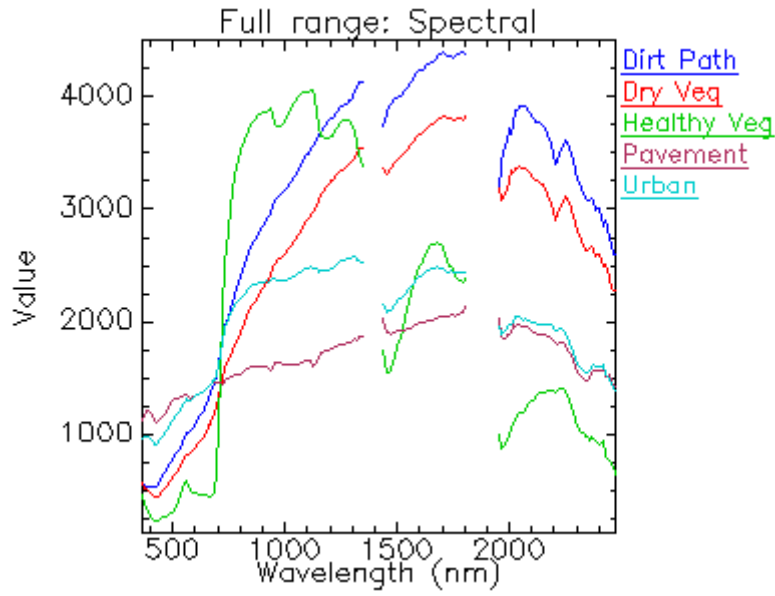


Figure 15. Full range: Spectral average for each ROI.

In Figure 16, the texture bands have been extracted from each spectral subset region of the full spectral range. The data range is approximately -10 to +500. Texture bands 1–15 (defined in Table 3) come from the average values of set one 365–928 nm, which is considered to be the visible to near IR region of the electromagnetic spectrum. Texture bands 16–30 (definitions are the same as bands 1–15) come from set two and so on. An interesting result is to note that the correlation texture features from set one, particularly for Dry Veg, are very strong compared to the rest, reaching a value of nearly 500 where the rest of the sets peak near 50.

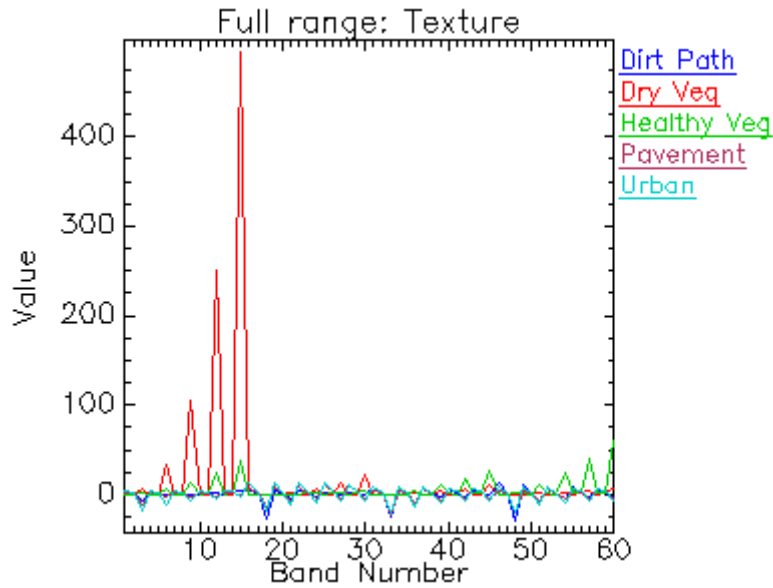


Figure 16. Full range: Texture average for each ROI.

We can see in Figure 17 the full range of texture features after the MNF transform and the removal of noise components. This MNF texture data have been scaled by a factor of 200 to match the spectral data. The data range is approximately -4100 to 3000. Comparing the two classes Dirt Path and Dry Veg, again we see a big difference from the spectral signatures. In this case, the Dry Veg has a local maximum at band six while Dirt Path shows a local minimum in the same band. This provides a clear distinction between these two classes which are spectrally very similar.

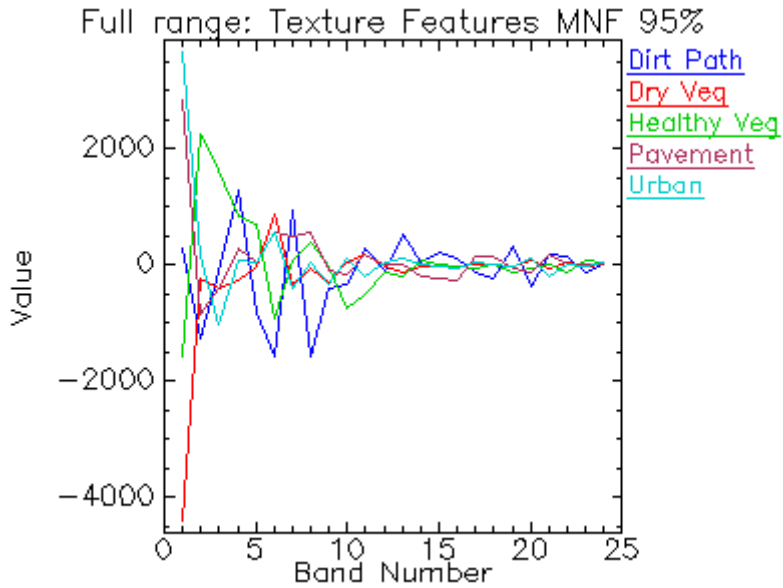


Figure 17. Full range: Texture average 95% MNF for each ROI.

B. CLASSIFICATION IMAGES

The classification images are the result of running the trained maximum likelihood classifier on the entire data set. A better result is one that better matches the ROIs, which are defined as ground truth. In this section, the images are shown side by side to get a sense of how they relate to each other. Larger sized images are shown separately in the Appendix to view finer details.

1. Set One: 365–928 nm

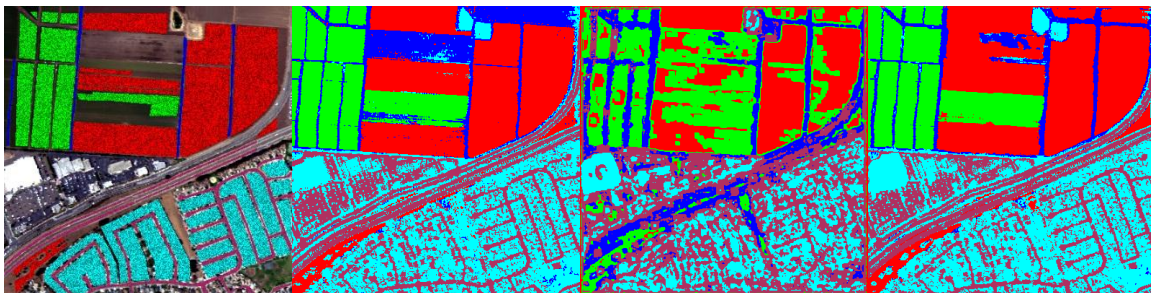


Figure 18. Set one classification images from left to right: (1) ROIs, (2) spectral-only, (3) texture-only, (4) spectral and texture.

2. Full Range: 365–2466 nm

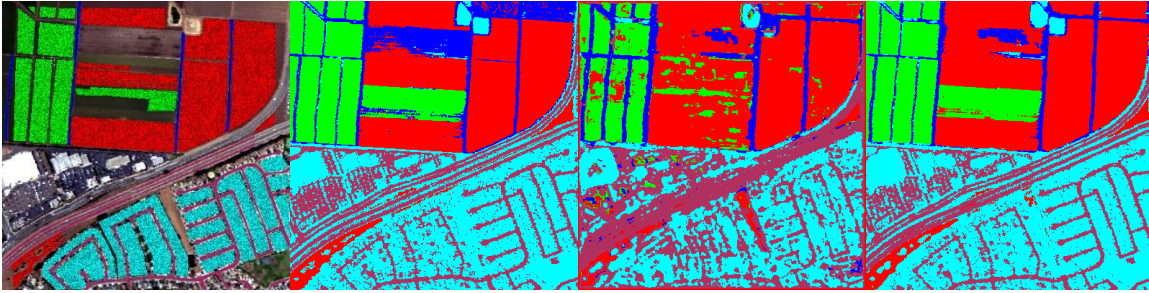


Figure 19. Full range classification images from left to right: (1) ROIs, (2) spectral-only, (3) texture-only, (4) spectral and texture.

C. CONFUSION MATRICES

To quantify the accuracy of the classifications confusion matrices were used to show how well the classifier does when compared to the pre-selected verification ROIs. Because the classifier was trained using a separate set of ROIs, these verification ROIs are independent and are not biased by the training process. These confusion matrices indicate what percent of the verification ROIs were correctly classified. Unclassified pixels, which include all pixels that were not assigned to either the training set of ROIs or the verification set of ROIs, were not included in the accuracy measurements. The reason for this approach is to, as clearly as possible, isolate the improvement of adding the additional texture features to the traditional spectral-only classification method. While excluding the unclassified pixels from the process means that every pixel will get assigned to one of the five classes, only the verification ROIs are used to assess accuracy.

1. Set One: 365–928 nm

Shown below in Table 6 is the confusion matrix for the set one spectral-only classification accuracy results. Dry Veg (near 99%), Healthy Veg (near 99%), Dirt Path (near 95%), and Pavement (near 91%) all classify very accurately using spectral data only. The Pavement class had near 9% false positives from the Urban class likely due to the Pavement class being found in

the Urban class area mixture. The Urban class had an accuracy of near 74% with near 25% false positives from the Pavement class. This is likely due to the presence of the Pavement class in the mixture that makes up the Urban class.

	Dry Veg	Healthy Veg	Urban	Dirt Path	Pavement
Dry Veg	99.37	0.00	0.01	2.76	0.00
Healthy Veg	0.00	99.11	0.01	1.10	0.00
Urban	0.16	0.01	74.28	1.38	8.86
Dirt Path	0.47	0.88	0.56	94.75	0.02
Pavement	0.00	0.00	25.14	0.00	91.11
Overall Accuracy	91.03				
Kappa	0.8770				

Table 6. Spectral-only confusion matrix results for set one.

Shown below in Table 7 is the confusion matrix for the set one texture-only classification accuracy results. Dry Veg had an accuracy of near 64% and near 31% were false positives from the Healthy Veg class, this shows there is some level of similarity between these two. The Healthy Veg class had an accuracy of near 75% with some (near 6%) false positives from Dry Veg but more (near 14%) false positives from the Dirt Path class. This shows that for this spectral range the texture of Healthy Veg is more like Dirt Path and Dry Veg is less like Dirt Path. It would seem that Dry Veg should share attributes with Dirt Path because the soil below the vegetation is more visible in the Dry Veg class. The accuracy of the Dirt Path class is near 92% with some (near 7%) false positives from the Pavement class, this is likely due to the relatively flat surface found in both classes. The accuracy of the Pavement class was found to be near 66% with false positives split between Urban (near 15%) and Dirt Path (near 14%). The false positives in the Urban class are likely due to the presence of Pavement in the mixture of components found in the Urban class.

	Dry Veg	Healthy Veg	Urban	Dirt Path	Pavement
Dry Veg	64.47	6.55	0.35	0.37	0.65
Healthy Veg	31.34	75.45	0.14	1.20	3.50
Urban	0.00	0.00	54.27	0.28	15.16
Dirt Path	2.94	14.17	0.45	91.62	14.27
Pavement	1.25	3.83	44.79	6.54	66.42
Overall Accuracy	64.47				
Kappa	0.5393				

Table 7. Texture-only confusion matrix results for set one.

Shown in Table 8 is the confusion matrix for the spectral and texture classification accuracy results. The Dry Veg (near 98%), Healthy Veg (near 99%), Dirt Path (near 97%), and Pavement (near 91%) accuracies are mostly the same as the spectral-only results. The Urban class had an accuracy near 78% for set one spectral and texture classification. This is up from near 74% and the false positives were near 21%, which is down from near 25%. This shows that the improvement in Urban classification comes directly from the largest false positive class. This result is promising because the improvement in accuracy did not spread out the false positives into the other classes.

	Dry Veg	Healthy Veg	Urban	Dirt Path	Pavement
Dry Veg	98.40	0.00	0.00	0.64	0.00
Healthy Veg	0.01	99.01	0.00	0.37	0.00
Urban	0.34	0.01	78.10	1.57	9.33
Dirt Path	1.25	0.98	0.22	97.15	0.00
Pavement	0.00	0.00	21.69	0.28	90.67
Overall Accuracy	91.76				
Kappa	0.8868				

Table 8. Spectral and texture confusion matrix results set one.

Table 9 is the combination of three confusion matrices and shows the results for spectral, texture, and the combined data sets. These are results for set one only and the remaining sets confusion matrices are included in the Appendix.

This combined data set will indicate the success of integration of the spectral and texture data sets. Looking at the spectral results, we can see a very high accuracy for the Dry Veg and Healthy Veg classes, and poorest results for the Urban class. Texture-only accuracy was reasonably good for all classes with the highest accuracy for the Dirt Path class. For the combined results, the Dry Veg and Healthy Veg classes suffered a small decrease in accuracy possible due to some correlation between the spectral data and the texture data or the addition of noise from the texture bands. Urban was the lowest performing class for spectral-only, but with the addition of texture made a significant improvement of nearly 4%. The Dirt Path class also made an improvement of nearly 2.5%.

	Spectral	Texture	Combined	Combined - Spectral
Dry Veg	99.37	64.47	98.40	-0.97
Healthy Veg	99.11	75.45	99.01	-0.10
Urban	74.28	54.27	78.10	3.82
Dirt Path	94.75	91.62	97.15	2.40
Pavement	91.11	66.42	90.67	-0.44
Overall	91.03	64.47	91.76	0.73
Kappa	0.8770	0.5393	0.8868	0.0098

Table 9. Summary of confusion matrix results for set one.

2. Full Range: 365–2466 nm

For the full range accuracy results all measures improved compared to the set one results. The Urban and Dirt Path classes still both improved with the addition of texture features but only by about 4% and 1.2% respectively. It appears that as the spectral-only classification accuracy approaches 100% it becomes harder for the additional texture features to improve upon the accuracy.

	Spectral	Texture	Combined	Combined - Spectral
Dry Veg	99.44	91.17	99.04	-0.40
Healthy Veg	99.46	76.33	99.27	-0.19
Urban	86.94	74.06	90.92	3.98
Dirt Path	96.69	96.50	97.88	1.19
Pavement	90.81	85.10	91.04	0.23
Overall	94.81	83.01	95.83	1.02
Kappa	0.9281	0.7677	0.9421	0.014

Table 10. Summary confusion matrix for full range.

D. CLASSIFICATION ACCURACY SUMMARY CHARTS

1. Spectral-Only Classification Accuracy

Shown below in Figure 21 are the accuracy results for the spectral-only classification. While the combination of all four regions did produce higher accuracy than any single spectral region, the most variation is seen in the Urban class. For the Urban class, set three showed the lowest performance at near 50%, while sets one and four did best at near 75%, and set two was in between near 64%.

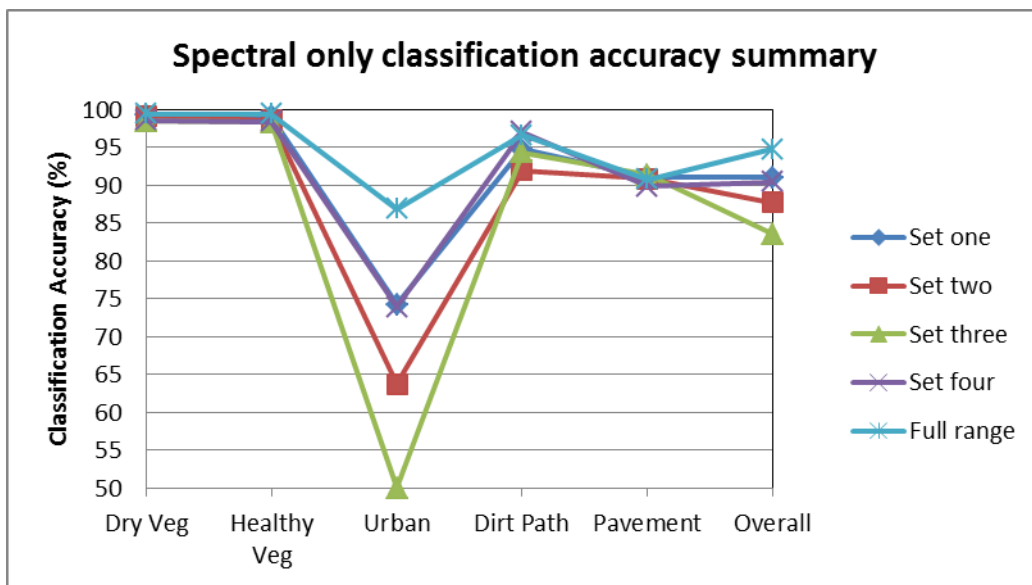


Figure 20. Spectral-only classification accuracy summary.

2. Texture-Only Classification Accuracy

Shown in Figure 21 is the classification accuracy summary for the texture-only data set. This chart displays results for each class and for each spectral range used for the texture feature analysis. For the Healthy Veg class, the set two spectral range was more accurate than any other spectral range or the full range. This is likely due to a large amount of noise present in the remaining spectral ranges. For the Dry Veg class, sets three and four did well with accuracies near 89%, and the least accurate spectral range was set two with near 30% accuracy. For the remaining classes Urban (near 55%), Dirt Path (near 85%), and Pavement (near 70%), the accuracies for each spectral range were within 10%.

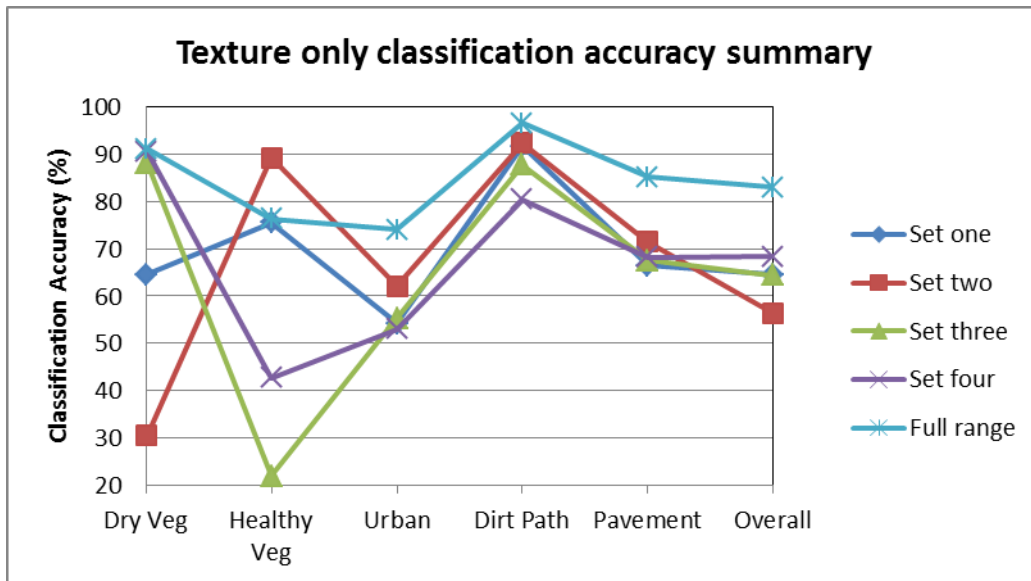


Figure 21. Texture-only classification accuracy summary.

3. Spectral and Texture Classification Accuracy

Shown in Figure 22 is the classification summary for the combined spectral and texture data set. The results of this data set are very similar to the spectral-only classification accuracy summary. The Urban class shows

improvement over the spectral-only data, but it still is the most varied, from near 60% for set three, to near 79% for sets one and four.

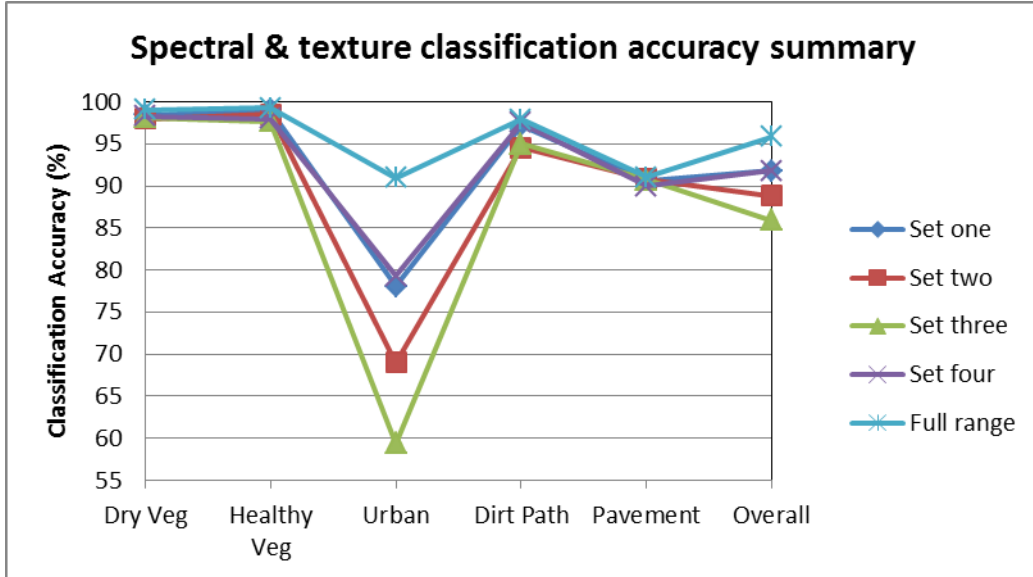


Figure 22. Spectral and texture classification accuracy summary.

V. SUMMARY AND CONCLUSIONS

A. SUMMARY

AVIRIS data collected over Salinas, CA and surrounding areas were used in this study as the source for both spectral processing and texture extraction. It has been shown that the addition of texture features to hyperspectral imagery can improve the classification accuracy of area targets. This was most significant in the Urban and Dirt Path classes, where an overall improved accuracy of approximately 4% and 2.5% respectively were shown. The accuracy of the Urban and Dirt Path classes, as they vary with analysis technique, are shown in Figures 23 and 24. respectively.

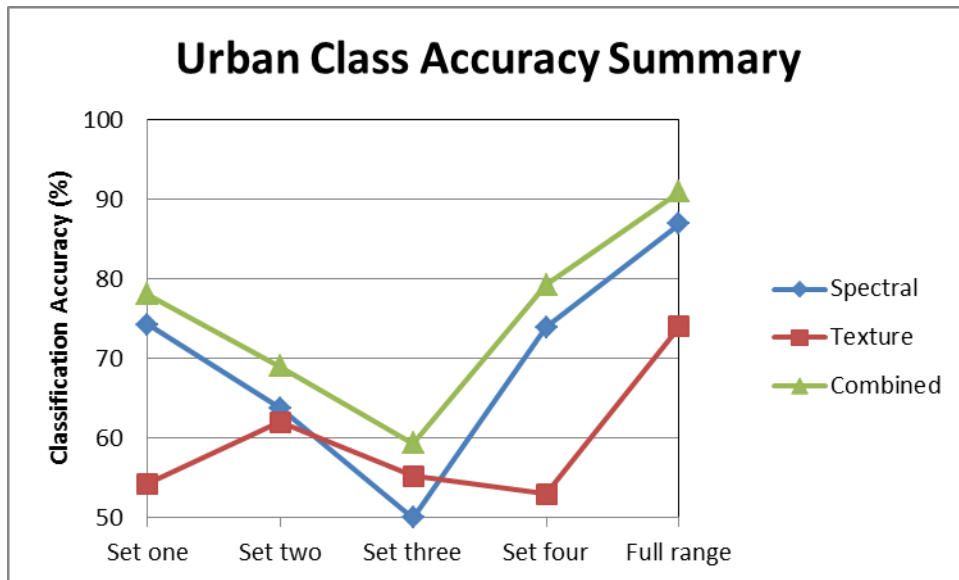


Figure 23. Urban classification accuracy summary. Optimal wavelength range set two (947–1343 nm).

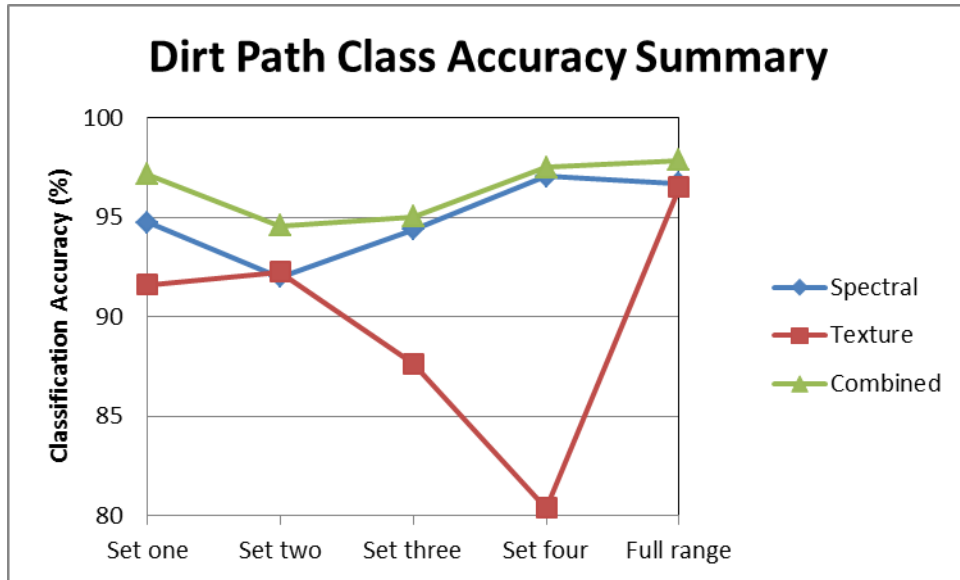


Figure 24. Dirt Path classification accuracy summary. Optimal wavelength range set two (947–1343 nm).

In other cases, like Healthy Veg, the spectral information provided classification accuracy greater than 99%. Attempting to improve upon this would require more study because the increase in noise and correlated data start to degrade the results. For the Healthy Veg class the accuracy actually went down by approximately 1%, which was the largest decrease seen during this study. The overall improvement across all five classes was nearly 1%.

Texture is effective in accurately classifying some classes. Dirt Path and Dry Veg were among the highest using texture-only, extracted from the full spectral range, with accuracies of approximately 97% and 91% respectively. Some of the individual spectral sets provided good classification accuracies, for example, the Healthy Veg class using spectral set two was near 89%. Also the Dry Veg class using spectral set three was near 88%.

B. CONCLUSIONS

This research has shown that the use of texture features in classification of hyperspectral data can improve the identification of area targets. It has also been shown that the accuracy of target classification is dependent on the

wavelength range from which the texture features are extracted. For the highest classification accuracy, the texture features should be extracted from: set three (1432–1801 nm) or four (1957–2466 nm) for Dry Veg, set one (365–928 nm) or two (947–1343 nm) for Healthy Veg, set two (947–1343 nm) for Urban, Dirt Path, and Pavement. The reason these spectral sets out perform other sets is that the composition of the target area varies uniquely from class to class. A class like Healthy Veg does well in set one (VIS-NIR) because the leaves reflect relatively strongly in the NIR but the ground absorbs relatively strongly in the same range, this leads to intensity variation, which is the basis of texture. This research demonstrates the effectiveness of texture features for more accurate analysis of hyperspectral data and the importance of selecting the correct spectral range used to extract these features.

THIS PAGE INTENTIONALLY LEFT BLANK

VI. FUTURE WORK

A. FINER SUBSETS OF THE SPECTRAL RANGE

In this study, the AVIRIS spectral range was divided into four spectral subsets. Further refinement might be obtained by dividing up this spectral range even further. This would allow for more specific spectral subsets to be used to improve the identification of specific area targets.

B. HIGHER SPATIAL RESOLUTION IMAGERY

The unique texture features that can be extracted from an image are limited to the resolution of the image. Features where the scale of the area target textures are smaller than the resolution become inaccessible from that image. Higher spatial resolution data should be explored, which will allow more area target classes to be examined.

C. OTHER TEXTURE MEASURES

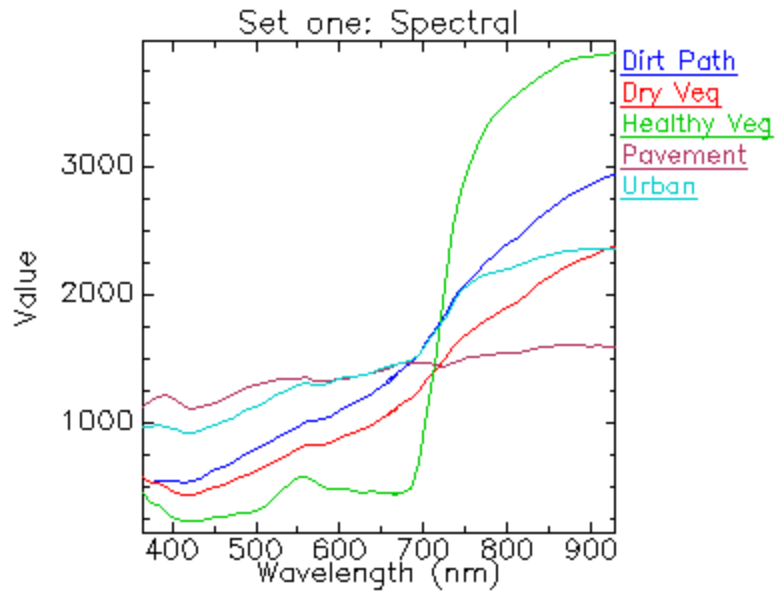
Alternative texture measure should be tried. The work done using texture units (He & Wang, 1990) is worth exploring. Computer code would need to be written to implement this method. The method is well laid out and the results shown are promising.

THIS PAGE INTENTIONALLY LEFT BLANK

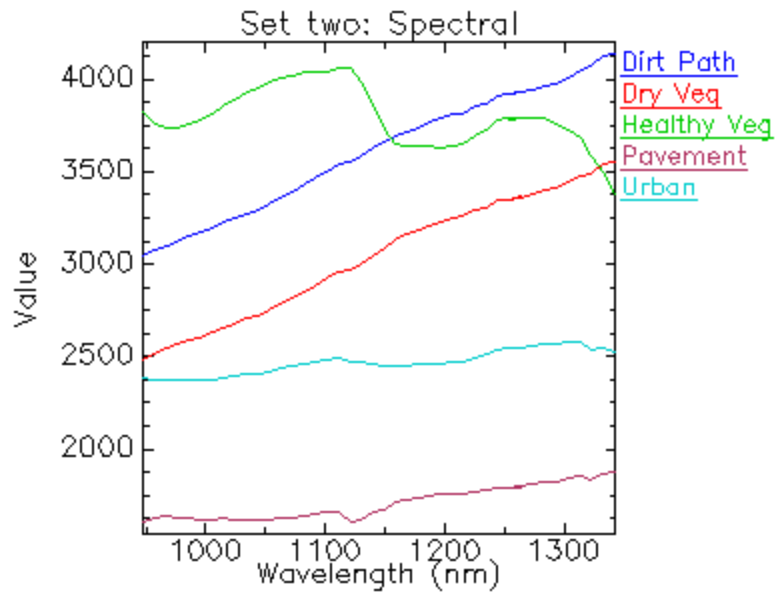
APPENDIX

A. SPECTRAL PLOTS

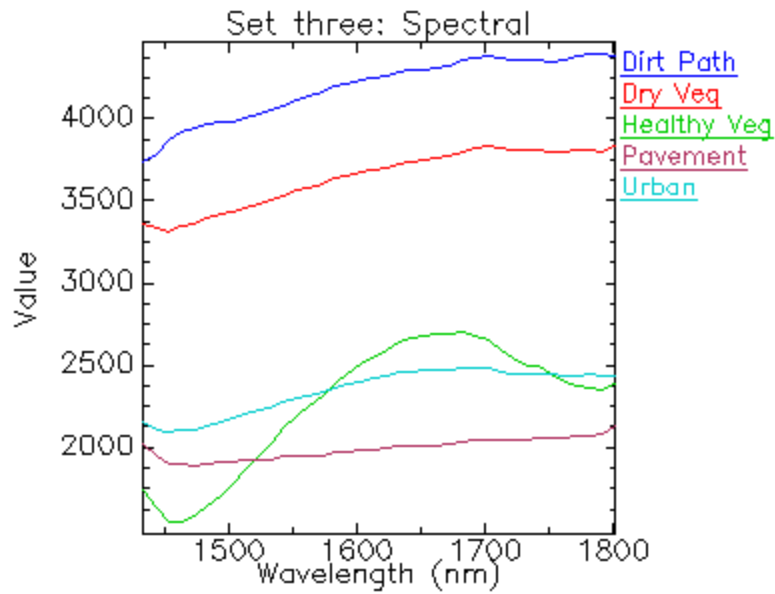
1. Set One: 365–928 nm



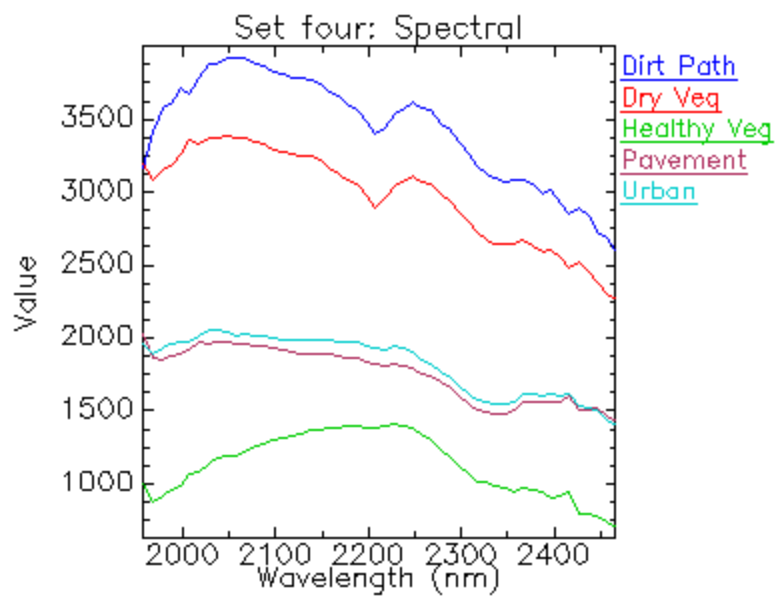
2. Set Two: 947–1343 nm



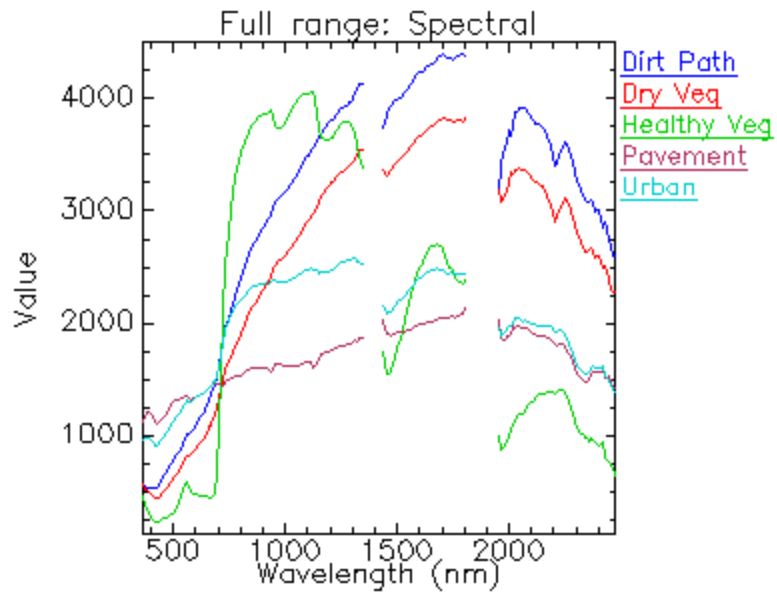
3. **Set Three: 1432–1801 nm**



4. **Set Four: 1957–2466 nm**



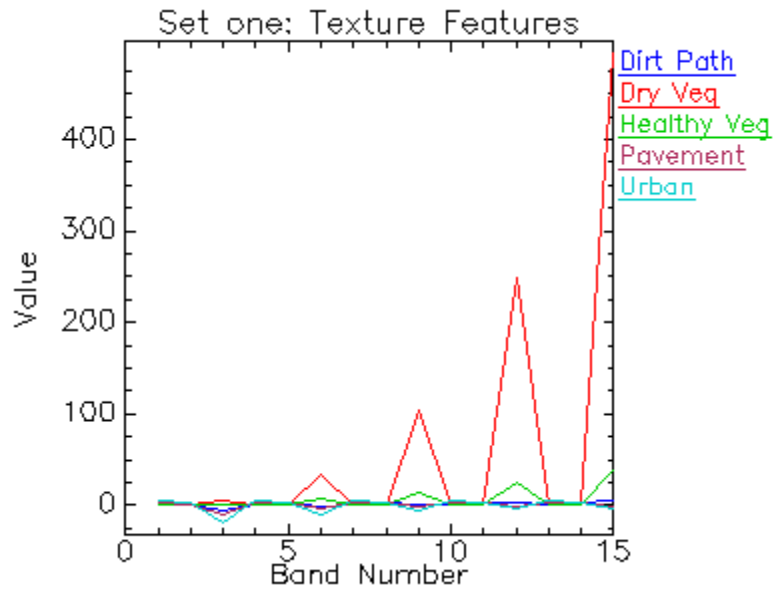
5. Full Range: 365–2466 nm



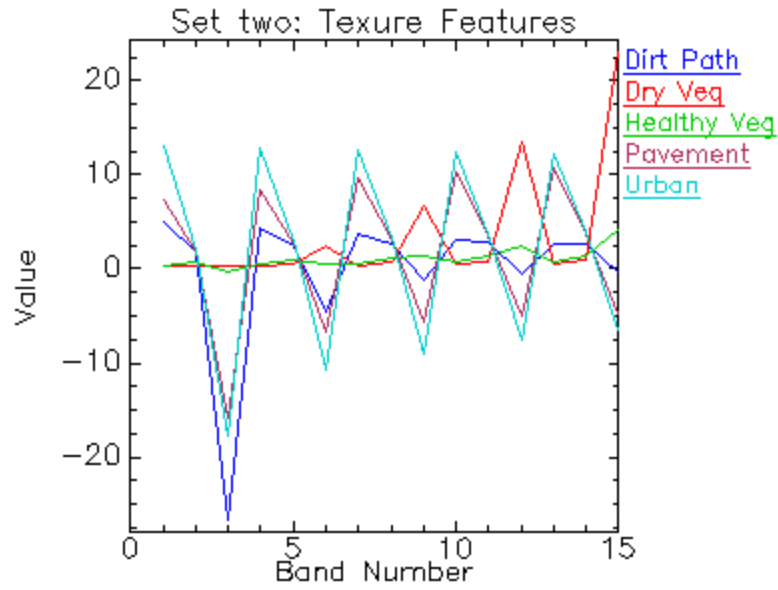
B. TEXTURE FEATURE PLOTS

For these texture feature plots the x-axis represents the texture band as described in Table 3. The y-axis is the value of each texture feature. In either case, there are no units that apply.

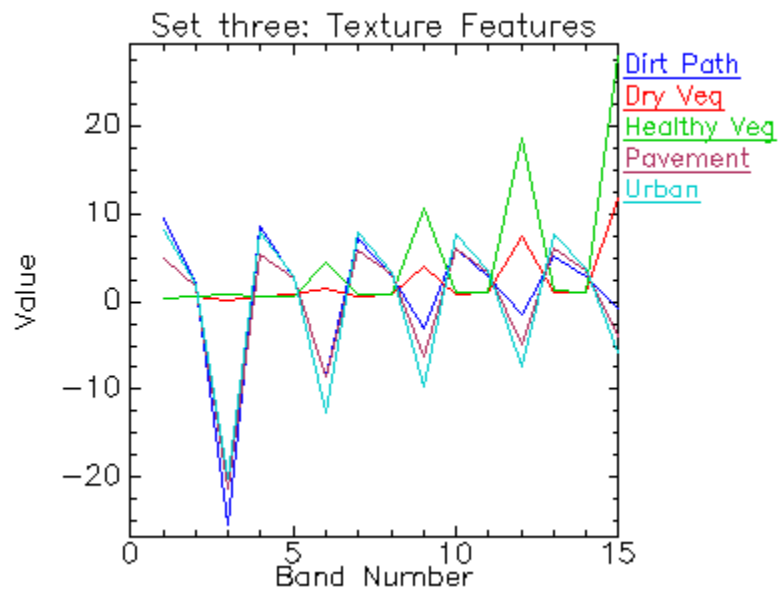
1. Set One: 365–928 nm



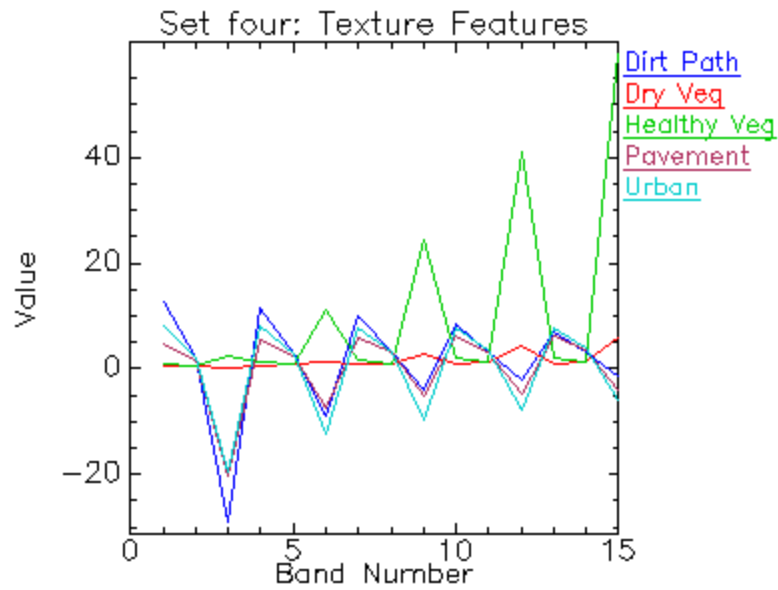
2. **Set Two: 947–1343 nm**



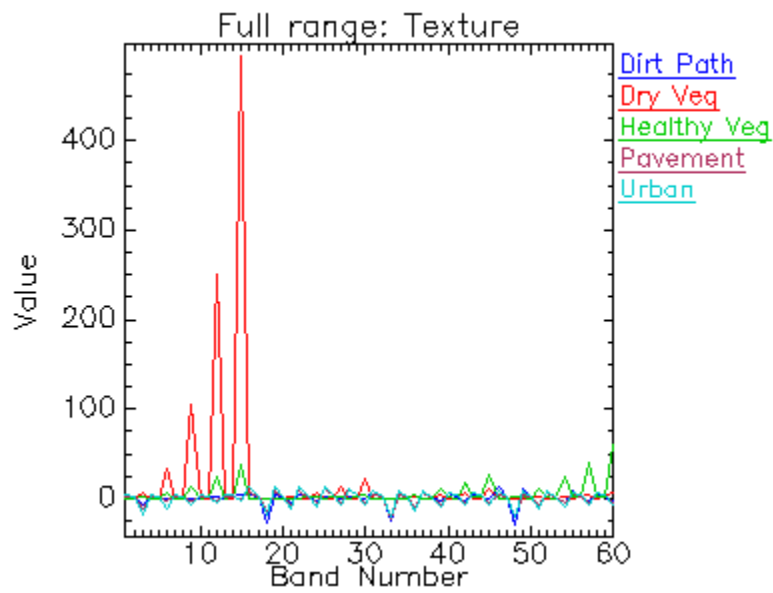
3. **Set Three: 1432–1801 nm**



4. **Set Four: 1957–2466 nm**



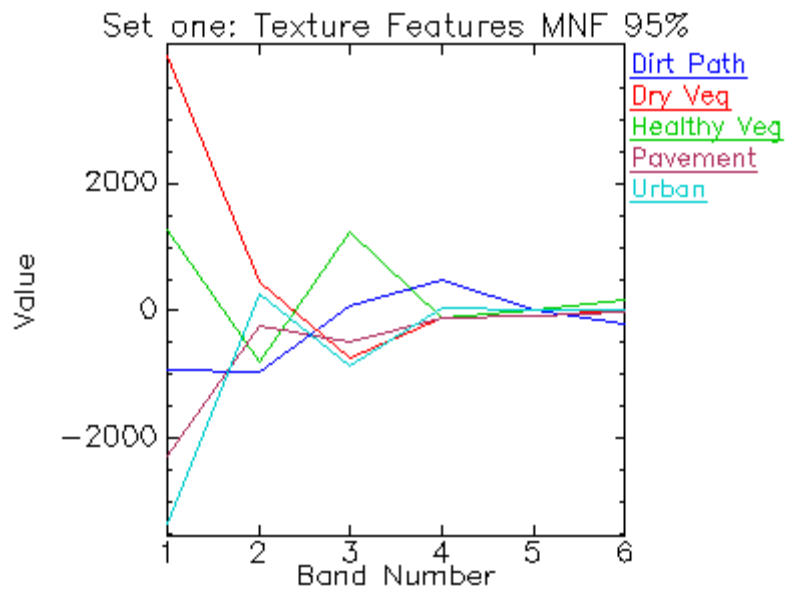
5. **Full Range: 365–2466 nm**



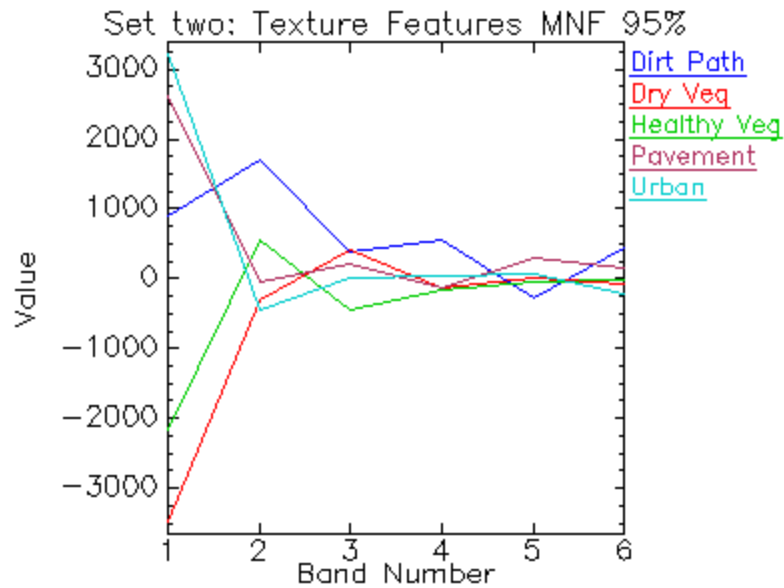
C. TEXTURE FEATURE MNF 95% PLOTS

For these texture feature plots the x-axis is the result of the dimensionality reduction and they related to the eigenvectors. The y-axis for these plots is the related to the eigenvalue multiplied by 200 to blend in better with the spectral data.

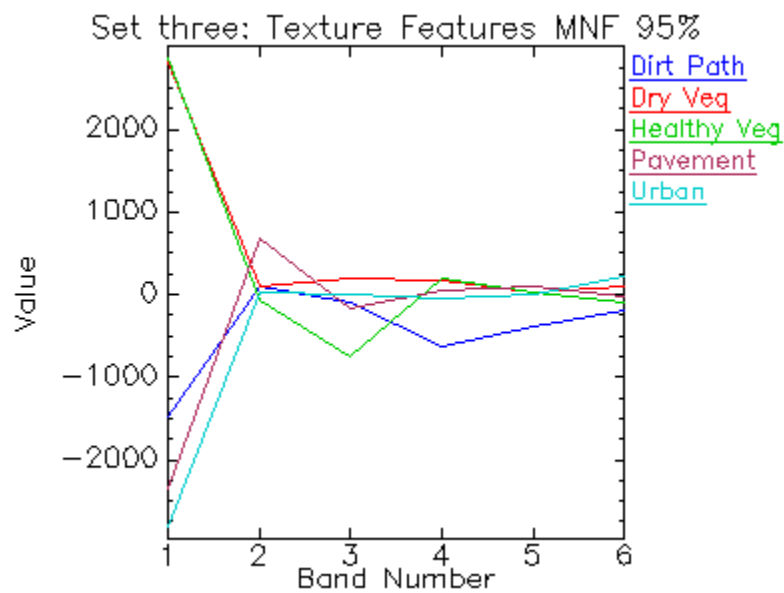
1. Set One: 365–928 nm



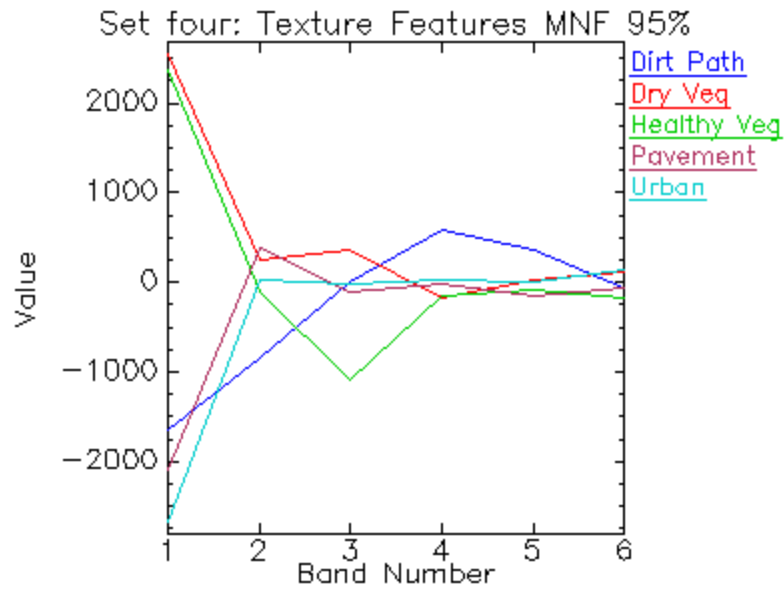
2. **Set Two: 947–1343 nm**



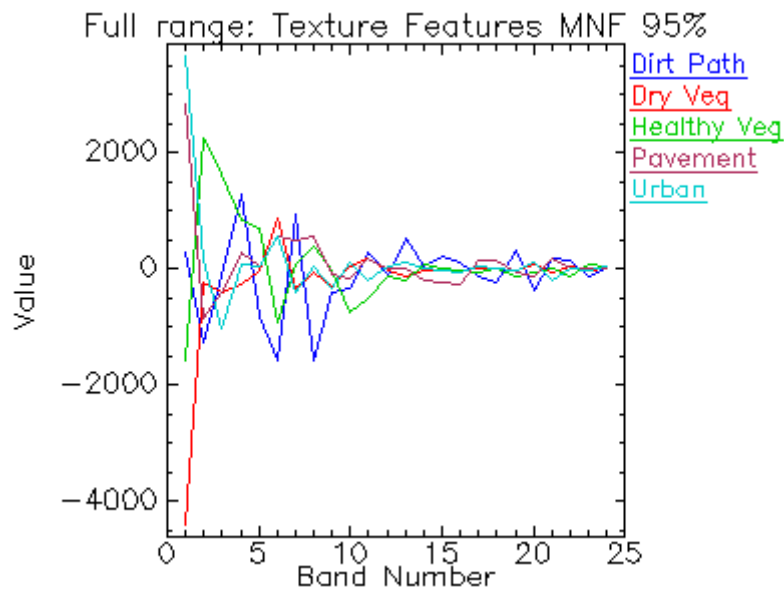
3. **Set Three: 1432–1801 nm**



4. **Set Four: 1957–2466 nm**



5. **Full Range: 365–2466 nm**



D. CLASSIFICATION IMAGES

1. Set One: 365–928 nm

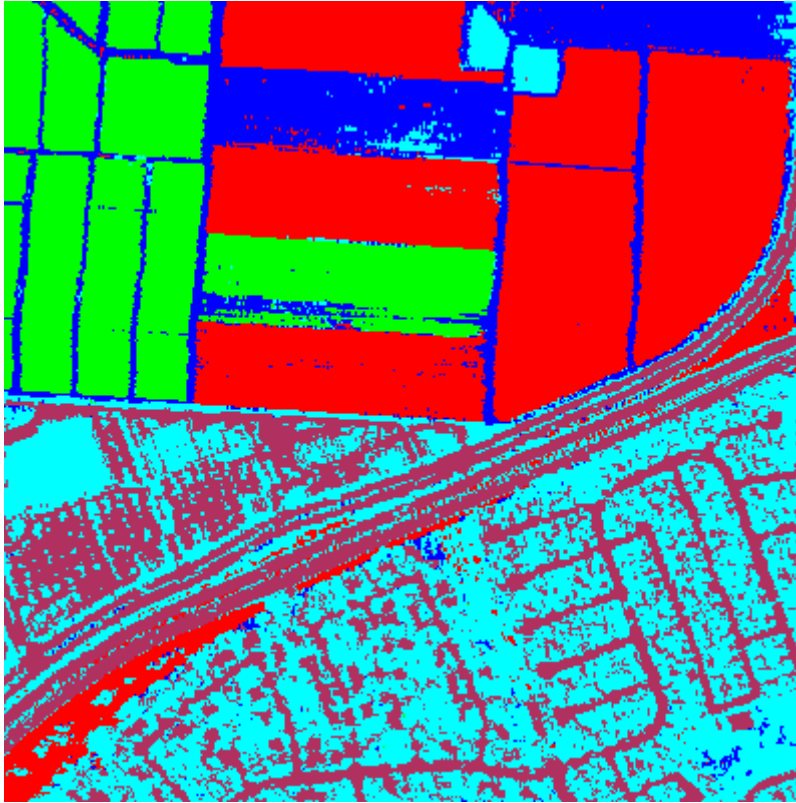


Figure 25. Full resolution spectral-only classification image set one.

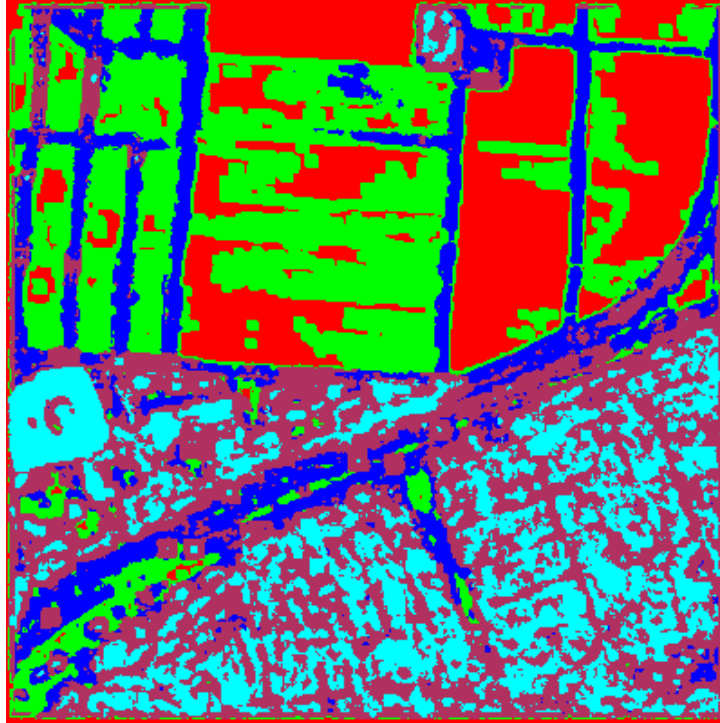


Figure 26. Full resolution texture-only classification image set one.

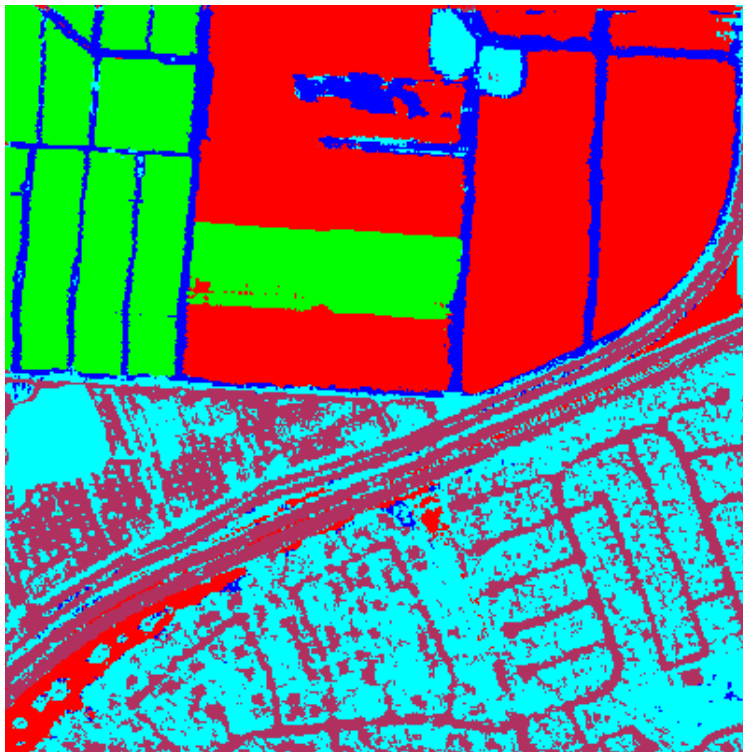


Figure 27. Full resolution spectral and texture classification image set one.

2. Set Two: 947–1343 nm

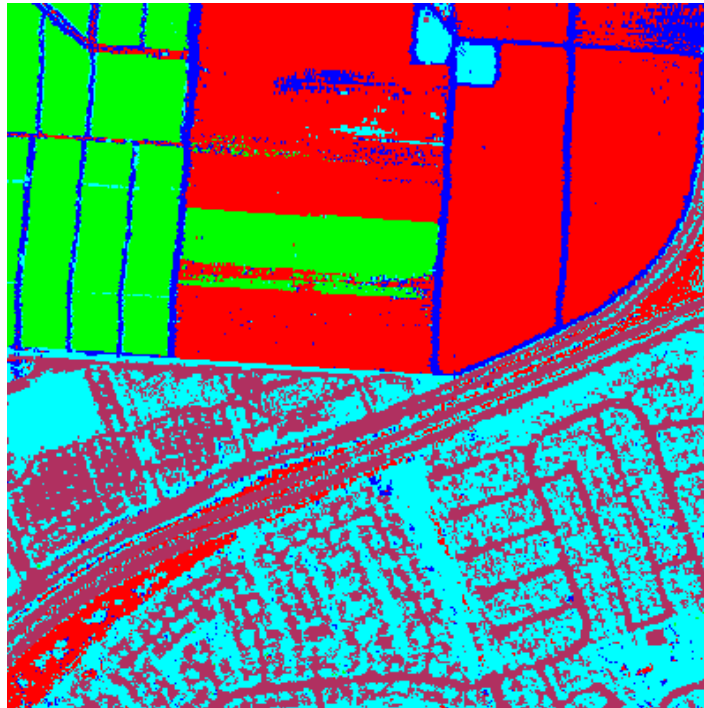


Figure 28. Full resolution spectral-only classification image set two.

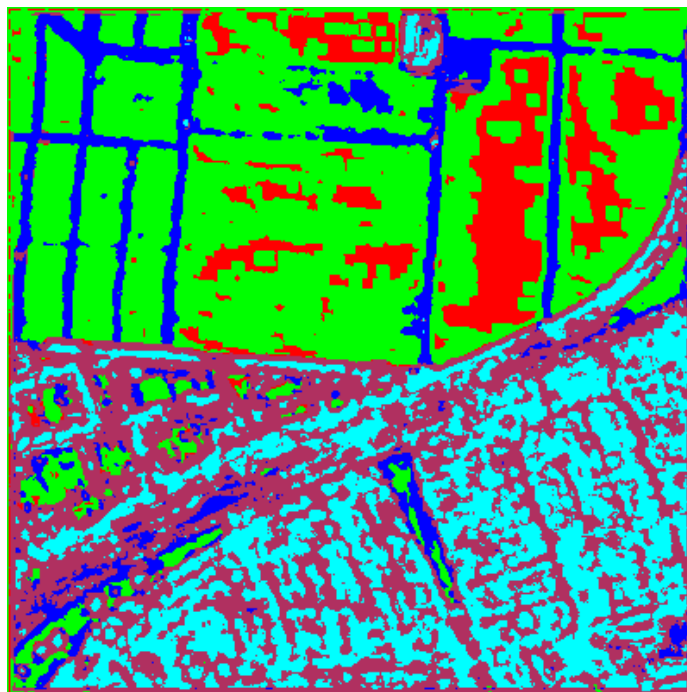


Figure 29. Full resolution texture-only classification image set two.

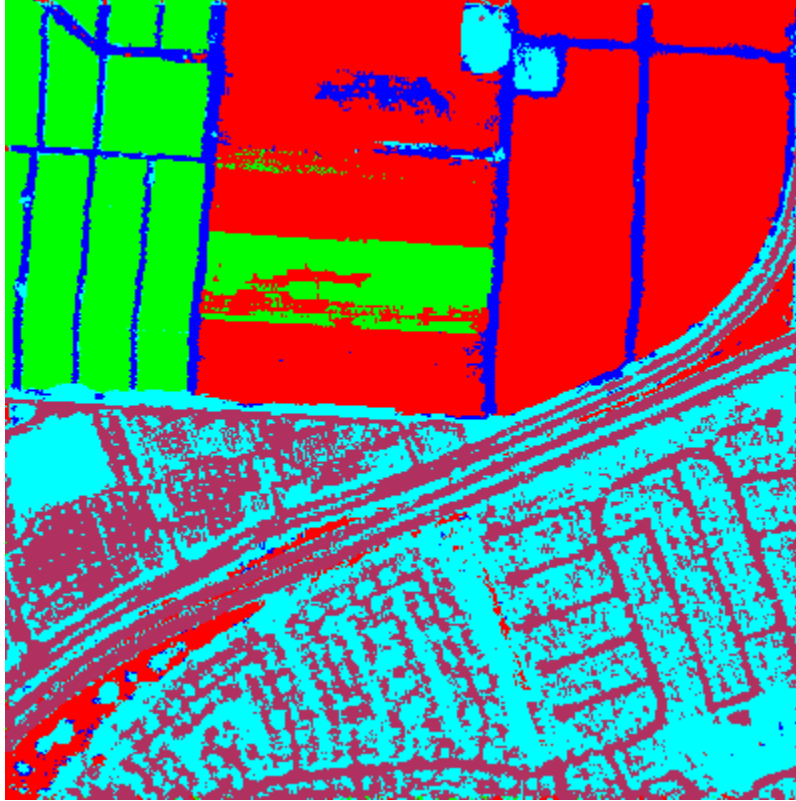


Figure 30. Full resolution spectral and texture classification image set two.

3. Set Three: 1432–1801 nm

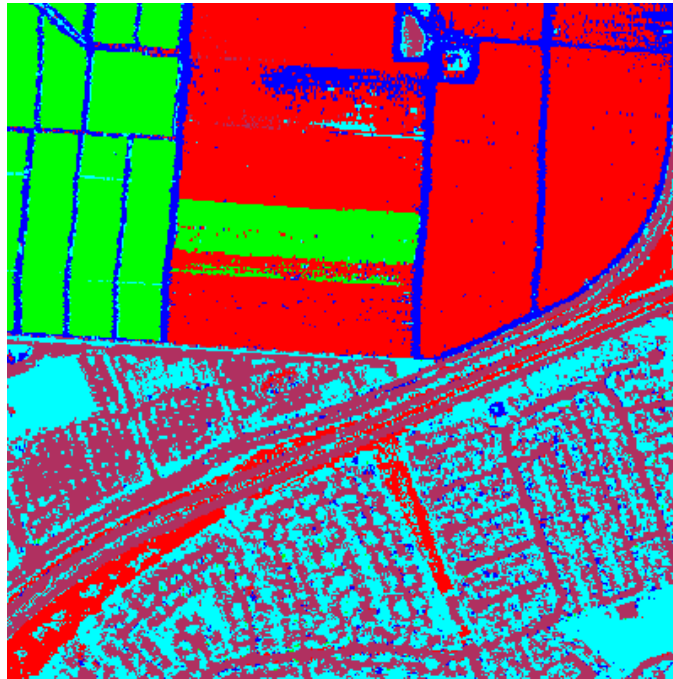


Figure 31. Full resolution spectral-only classification image set three.

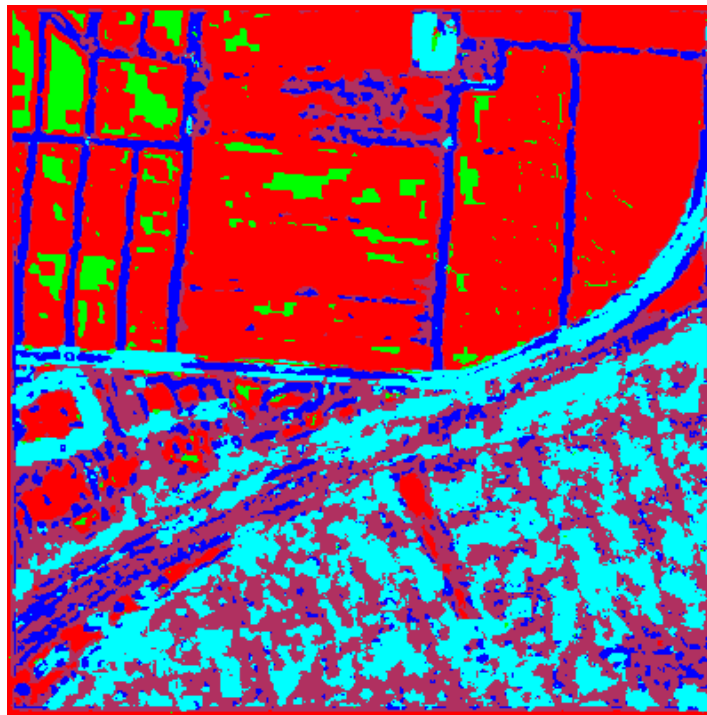


Figure 32. Full resolution texture-only classification image set three.

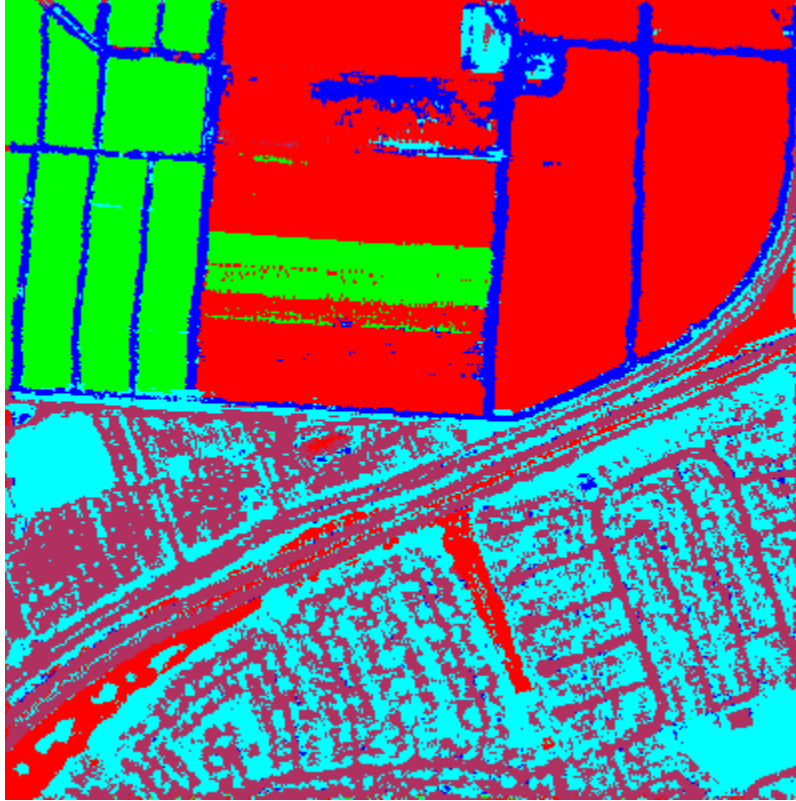


Figure 33. Full resolution spectral and texture classification image set three.

4. Set Four: 1957–2466 nm

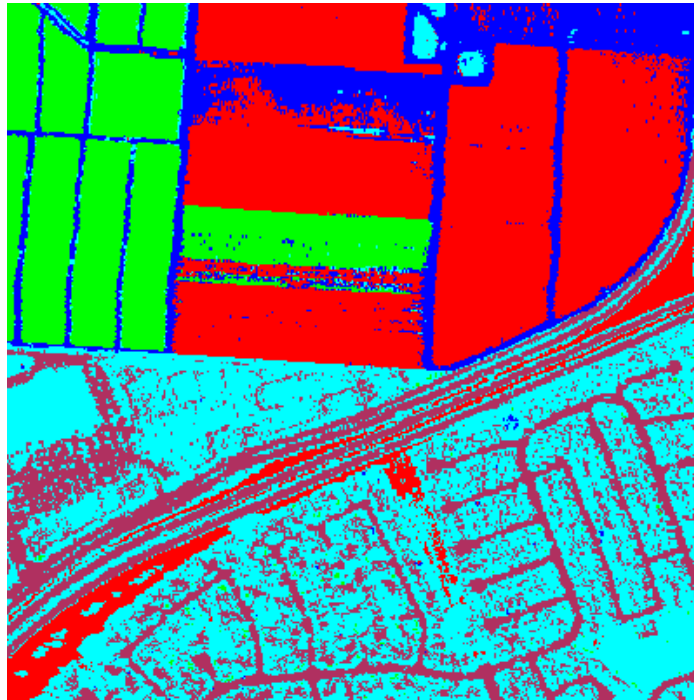


Figure 34. Full resolution spectral-only classification image set four.

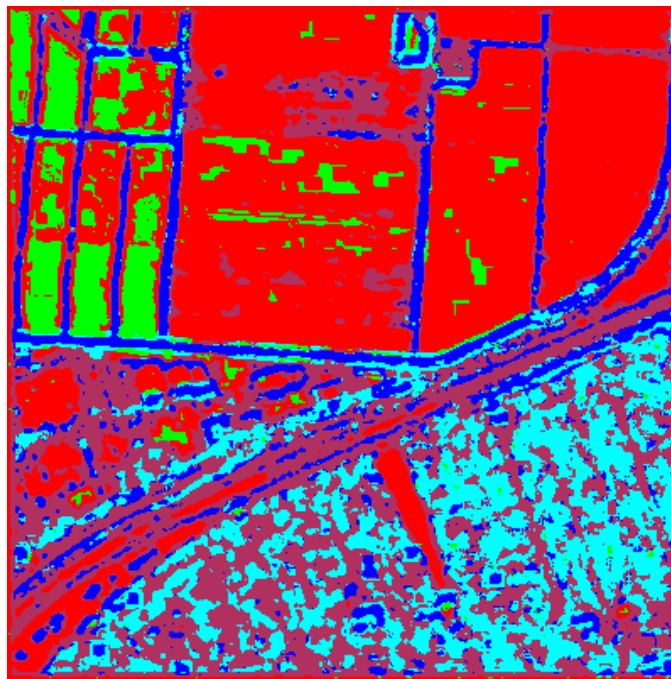


Figure 35. Full resolution texture-only classification image set four.

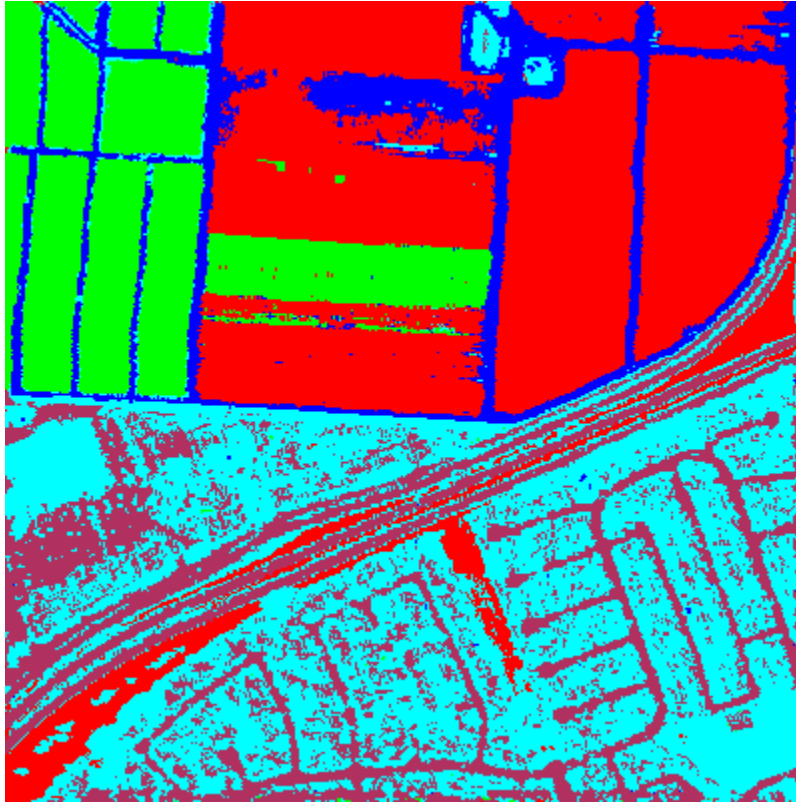


Figure 36. Full resolution spectral and texture classification image set four.

5. Full Range: 365–2466 nm

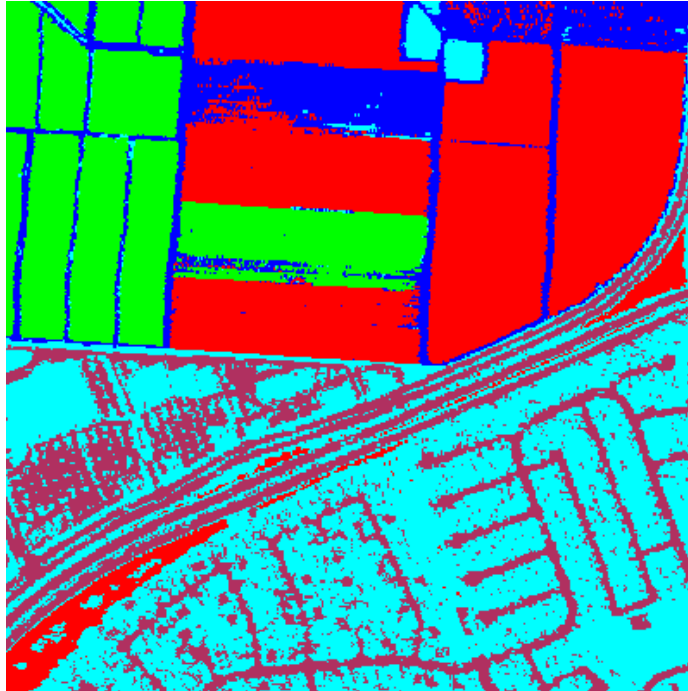


Figure 37. Full resolution spectral-only classification image full range.

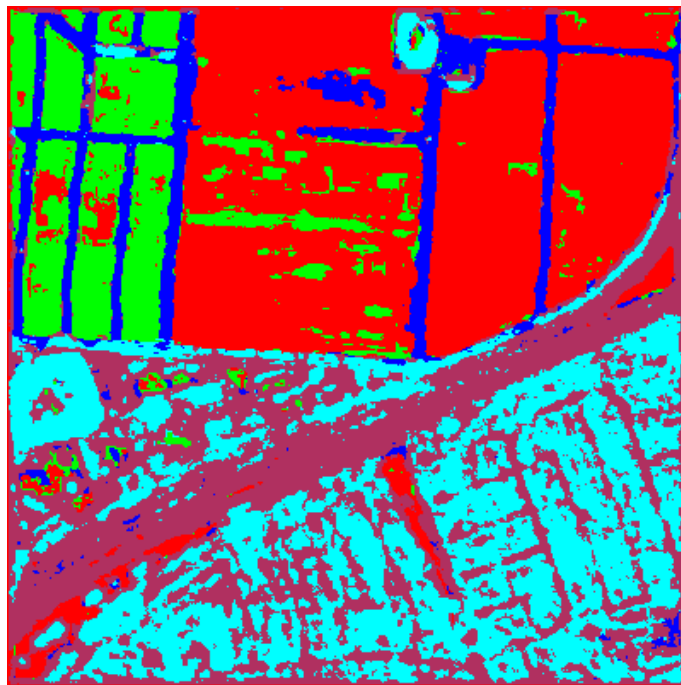


Figure 38. Full resolution texture-only classification image full range.

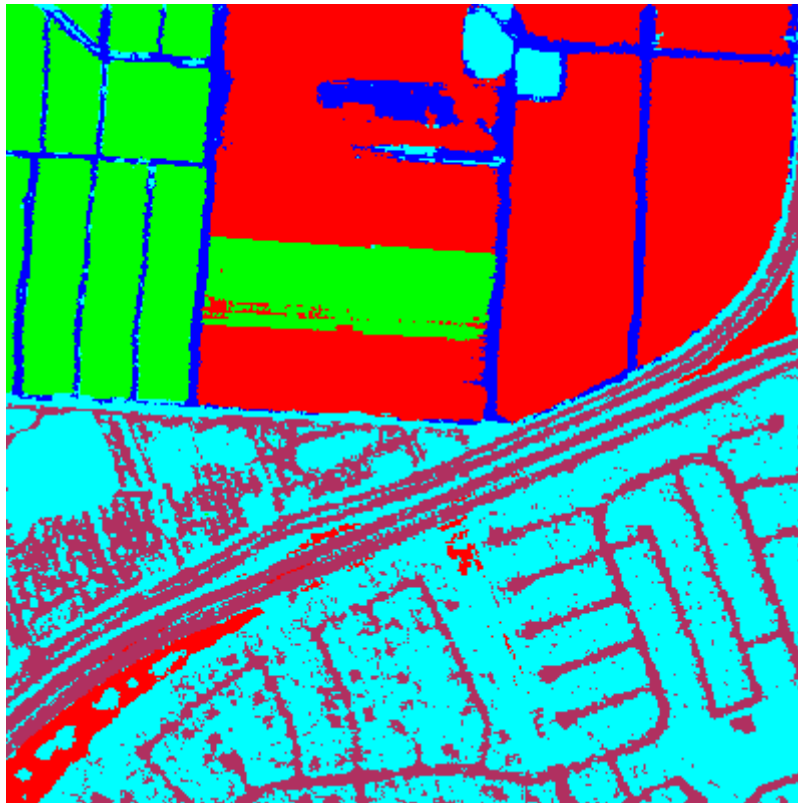


Figure 39. Full resolution spectral and texture classification image full range.

E. CONFUSION MATRICES

1. Set One: 365–928 nm

	Dry Veg	Healthy Veg	Urban	Dirt Path	Pavement
Dry Veg	99.37	0.00	0.01	2.76	0.00
Healthy Veg	0.00	99.11	0.01	1.10	0.00
Urban	0.16	0.01	74.28	1.38	8.86
Dirt Path	0.47	0.88	0.56	94.75	0.02
Pavement	0.00	0.00	25.14	0.00	91.11
Overall Accuracy	91.03				
Kappa	0.8770				

Table 11. Spectral-only confusion matrix set one.

	Dry Veg	Healthy Veg	Urban	Dirt Path	Pavement
Dry Veg	64.47	6.55	0.35	0.37	0.65
Healthy Veg	31.34	75.45	0.14	1.20	3.50
Urban	0.00	0.00	54.27	0.28	15.16
Dirt Path	2.94	14.17	0.45	91.62	14.27
Pavement	1.25	3.83	44.79	6.54	66.42
Overall Accuracy	64.47				
Kappa	0.5393				

Table 12. Texture-only confusion matrix set one.

	Dry Veg	Healthy Veg	Urban	Dirt Path	Pavement
Dry Veg	98.40	0.00	0.00	0.64	0.00
Healthy Veg	0.01	99.01	0.00	0.37	0.00
Urban	0.34	0.01	78.10	1.57	9.33
Dirt Path	1.25	0.98	0.22	97.15	0.00
Pavement	0.00	0.00	21.69	0.28	90.67
Overall Accuracy	91.76				
Kappa	0.8868				

Table 13. Spectral and texture confusion matrix set one.

	Spectral	Texture	Combined	Combined - Spectral
Dry Veg	99.37	64.47	98.40	-0.97
Healthy Veg	99.11	75.45	99.01	-0.10
Urban	74.28	54.27	78.10	3.82
Dirt Path	94.75	91.62	97.15	2.40
Pavement	91.11	66.42	90.67	-0.44
Overall	91.03	64.47	91.76	0.73
Kappa	0.8770	0.5393	0.8868	0.0098

Table 14. Summary of confusion matrix results for set one.

2. Set Two: 947–1343 nm

	Dry Veg	Healthy Veg	Urban	Dirt Path	Pavement
Dry Veg	99.17	0.00	0.29	4.97	0.02
Healthy Veg	0.01	98.62	0.07	1.20	0.00
Urban	0.36	0.68	63.78	1.84	9.00
Dirt Path	0.45	0.70	0.70	91.99	0.07
Pavement	0.00	0.00	35.16	0.00	90.90
Overall Accuracy	87.73				
Kappa	0.8327				

Table 15. Spectral-only confusion matrix set two.

	Dry Veg	Healthy Veg	Urban	Dirt Path	Pavement
Dry Veg	30.45	2.98	0.23	0.28	0.70
Healthy Veg	64.12	89.26	0.33	1.38	0.70
Urban	0.01	0.00	62.03	2.03	23.79
Dirt Path	2.69	6.53	0.05	92.27	3.38
Pavement	2.73	1.24	37.35	4.05	71.43
Overall Accuracy	56.44				
Kappa	0.4499				

Table 16. Texture-only confusion matrix set two.

	Dry Veg	Healthy Veg	Urban	Dirt Path	Pavement
Dry Veg	98.00	0.00	0.02	1.01	0.00
Healthy Veg	0.00	98.48	0.00	0.55	0.00
Urban	0.84	0.67	69.00	3.87	9.17
Dirt Path	1.16	0.85	0.00	94.57	0.00
Pavement	0.00	0.00	30.98	0.00	90.83
Overall Accuracy	88.81				
Kappa	0.8473				

Table 17. Spectral and texture confusion matrix set two.

	Spectral	Texture	Combined	Combined - Spectral
Dry Veg	99.17	30.45	98.00	-1.17
Healthy Veg	98.62	89.26	98.48	-0.14
Urban	63.78	62.03	69.00	5.22
Dirt Path	91.99	92.27	94.57	2.58
Pavement	90.90	71.43	90.83	-0.07
Overall	87.73	56.44	88.81	1.08
Kappa	0.8327	0.4499	0.8473	0.0146

Table 18. Summary of confusion matrix results for set two.

3. Set Three: 1432–1801 nm

	Dry Veg	Healthy Veg	Urban	Dirt Path	Pavement
Dry Veg	98.55	0.03	0.55	1.93	0.28
Healthy Veg	0.01	98.38	0.26	0.92	0.02
Urban	0.40	0.57	50.03	2.76	7.98
Dirt Path	0.92	1.02	3.24	94.38	0.33
Pavement	0.13	0.00	45.91	0.00	91.39
Overall Accuracy	83.58				
Kappa	0.7788				

Table 19. Spectral-only confusion matrix set three.

	Dry Veg	Healthy Veg	Urban	Dirt Path	Pavement
Dry Veg	88.15	71.69	0.61	0.83	1.26
Healthy Veg	4.90	21.91	0.10	0.28	0.05
Urban	1.49	1.08	55.28	4.60	20.85
Dirt Path	1.14	2.85	2.97	87.66	10.28
Pavement	4.32	2.47	41.04	6.63	67.56
Overall Accuracy	64.35				
Kappa	0.5052				

Table 20. Texture-only confusion matrix set three.

	Dry Veg	Healthy Veg	Urban	Dirt Path	Pavement
Dry Veg	98.11	0.07	0.04	0.92	0.00
Healthy Veg	0.01	97.67	0.03	0.28	0.00
Urban	0.58	0.63	59.34	3.41	8.96
Dirt Path	1.26	1.63	0.71	95.03	0.28
Pavement	0.05	0.00	39.88	0.37	90.76
Overall Accuracy	85.92				
Kappa	0.8093				

Table 21. Spectral and texture confusion matrix set three.

	Spectral	Texture	Combined	Combined - Spectral
Dry Veg	98.55	88.15	98.11	-0.44
Healthy Veg	98.38	21.91	97.67	-0.71
Urban	50.03	55.28	59.34	9.31
Dirt Path	94.38	87.66	95.03	0.65
Pavement	91.39	67.56	90.76	-0.63
Overall	83.58	64.35	85.92	2.34
Kappa	0.7788	0.5052	0.8093	0.0305

Table 22. Summary of confusion matrix results for set three.

4. Set Four: 1957–2466 nm

	Dry Veg	Healthy Veg	Urban	Dirt Path	Pavement
Dry Veg	98.60	0.00	0.05	1.20	0.00
Healthy Veg	0.01	98.42	0.71	0.83	0.00
Urban	0.19	0.52	73.97	0.92	10.07
Dirt Path	1.20	1.06	0.16	97.05	0.05
Pavement	0.00	0.00	25.11	0.00	89.88
Overall Accuracy	90.45				
Kappa	0.8691				

Table 23. Spectral-only confusion matrix set four.

	Dry Veg	Healthy Veg	Urban	Dirt Path	Pavement
Dry Veg	90.58	48.25	0.60	0.92	2.08
Healthy Veg	3.47	42.62	0.47	1.01	0.09
Urban	0.72	1.02	52.96	5.80	18.42
Dirt Path	1.03	2.99	6.17	80.39	11.26
Pavement	4.19	5.13	39.80	11.88	68.14
Overall Accuracy	68.26				
Kappa	0.5652				

Table 24. Texture-only confusion matrix set four.

	Dry Veg	Healthy Veg	Urban	Dirt Path	Pavement
Dry Veg	98.26	0.01	0.00	1.20	0.00
Healthy Veg	0.04	98.00	0.02	0.37	0.00
Urban	0.18	0.74	79.28	0.92	9.98
Dirt Path	1.53	1.24	0.04	97.51	0.05
Pavement	0.00	0.00	20.66	0.00	89.97
Overall Accuracy	91.79				
Kappa	0.8872				

Table 25. Spectral and texture confusion matrix set four.

	Spectral	Texture	Combined	Combined - Spectral
Dry Veg	98.60	90.58	98.26	-0.34
Healthy Veg	98.42	42.62	98.00	-0.42
Urban	73.97	52.96	79.28	5.31
Dirt Path	97.05	80.39	97.51	0.46
Pavement	89.88	68.14	89.97	0.09
Overall	90.45	68.26	91.79	1.34
Kappa	0.8691	0.5652	0.8872	0.0181

Table 26. Summary of confusion matrix results for set four.

5. Full Range: 365–2466 nm

	Dry Veg	Healthy Veg	Urban	Dirt Path	Pavement
Dry Veg	99.44	0.00	0.00	1.66	0.00
Healthy Veg	0.00	99.46	0.00	1.01	0.00
Urban	0.17	0.06	86.94	0.64	9.19
Dirt Path	0.39	0.49	0.00	96.69	0.00
Pavement	0.00	0.00	13.06	0.00	90.81
Overall Accuracy	94.81				
Kappa	0.9281				

Table 27. Spectral-only confusion matrix full range.

	Dry Veg	Healthy Veg	Urban	Dirt Path	Pavement
Dry Veg	91.17	15.72	0.33	0.83	0.47
Healthy Veg	3.54	76.33	0.00	0.00	0.00
Urban	0.59	0.13	74.06	1.29	14.37
Dirt Path	1.84	6.93	0.00	96.50	0.07
Pavement	2.86	0.89	25.61	1.38	85.10
Overall Accuracy	83.01				
Kappa	0.7677				

Table 28. Texture-only confusion matrix full range.

	Dry Veg	Healthy Veg	Urban	Dirt Path	Pavement
Dry Veg	99.04	0.00	0.00	0.55	0.00
Healthy Veg	0.00	99.27	0.00	0.37	0.00
Urban	0.43	0.07	90.92	1.20	8.96
Dirt Path	0.52	0.66	0.00	97.88	0.00
Pavement	0.00	0.00	9.08	0.00	91.04
Overall Accuracy	95.83				
Kappa	0.9421				

Table 29. Spectral and texture confusion matrix full range.

	Spectral	Texture	Combined	Combined - Spectral
Dry Veg	99.44	91.17	99.04	-0.40
Healthy Veg	99.46	76.33	99.27	-0.19
Urban	86.94	74.06	90.92	3.98
Dirt Path	96.69	96.50	97.88	1.19
Pavement	90.81	85.10	91.04	0.23
Overall	94.81	83.01	95.83	1.02
Kappa	0.9281	0.7677	0.9421	0.014

Table 30. Summary of confusion matrix results for full range.

LIST OF REFERENCES

- Andrews, H., Tescher, A., & Kruger, R. (1972). Image processing by digital-computer. *IEEE Spectrum*, 9(7) (Jul), 20–32.
- Bernstein, L., Adler-Golden, S., Sundberg, R., & Ratkowski, A. (2008). In-scene-based atmospheric correction of uncalibrated VISible-SWIR (VIS-SWIR) hyper- and multi-spectral imagery. *SPIE Proceedings*, Vol 7107.
- Bernstein, L., Jin, X., Gregor, B., & Adler-Golden, S. (2012). Quick atmospheric correction code: Algorithm description and recent upgrades. *Optical Engineering*, 51(11), 111719, 1–11.
- Bernstein, L., Adler-Golden, S., Sundberg, R., Levine, R., Perkins, T., Berk, A., et al. (2005). A new method for atmospheric correction and aerosol optical property retrieval for VIS-SWIR multi- and hyperspectral imaging sensors: QUAC (QUick Atmospheric Correction). IGARSS IEEE 2005 Proceedings, 3549–3552.
- Bernstein, L., Adler-Golden, S., Sundberg, R., Levine, R., Perkins, T., Berk, A., Ratkowski, A., & Hoke, M. (2004). A new method for atmospheric correction and aerosol property retrieval for VIS-SWIR multi- and hyperspectral imaging sensors: QUAC (QUick Atmospheric Correction). *Proceedings of the 2004 AVIRIS Workshop*.
- Bhatta, B. (2009). Analysis of urban growth pattern using remote sensing and GIS: A case study of Kolkata, India. *International Journal of Remote Sensing*, 30(18) (Sep), 4733–46.
- Boardman, J., & Kruse, F. (2011). Analysis of imaging spectrometer data using N-dimensional geometry and a mixture-tuned matched filtering approach. *IEEE Transactions on Geoscience and Remote Sensing* 49 (11) (Nov), 4138–52.
- Chai, S., Gentile, A., Lugo-Beauchamp, W., Fonseca, J., Cruz-Rivera, J., & Wills, D. (2000). Focal-plane processing architectures for real-time hyperspectral image processing. *Applied Optics*, 39(5) (Feb), 835–49.
- Clausi, D. (2002). An analysis of co-occurrence texture statistics as a function of grey level quantization. *Canadian Journal of Remote Sensing*, 28(1) (Feb), 45–62.
- Cloutis, E. (1996). Hyperspectral geological remote sensing: Evaluation of analytical techniques. *International Journal of Remote Sensing*, 17(12) (Apr), 2215–42.
- Coburn, C., & Roberts, A. (2004). A multiscale texture analysis procedure for improved forest stand classification. *International Journal of Remote Sensing*, 25(20) (Oct), 4287–308.

- Dalponte, M., Bruzzone, L., & Gianelle, D. (2008). Fusion of hyperspectral and LIDAR remote sensing data for classification of complex forest areas. *IEEE Transactions on Geoscience and Remote Sensing*, 46(5) (May), 1416–27.
- Dalponte, M., Bruzzone, L., & Gianelle, D. (2009). *Fusion of hyperspectral and lidar remote sensing data for the estimation of tree stem diameters*. IGARSS IEEE 2009 Proceedings, Vol 2, 1008–11.
- Foody, G. (2002). Status of land cover classification accuracy assessment. *Remote Sensing of Environment*. 80(1) (Apr): 185–201.
- Franklin, S., & Peddle, D. (1989). Spectral texture for improved class discrimination in complex terrain. *International Journal of Remote Sensing*, 10(8) (Oct), 1437–43.
- Franklin, S., & Wulder, M. (2002). Remote sensing methods in medium spatial resolution satellite data land cover classification of large areas. *Progress in Physical Geography*, 26(2), 173–205.
- Goetz, A., Vane, G., Solomon, J., & Rock, B. (1985). Imaging spectrometry for earth remote-sensing. *Science*, 228(4704) (Jun), 1147–53.
- Gong, P., Marceau, D., & Howarth, P. (1992). A comparison of spatial feature-extraction algorithms for land-use classification with SPOT HRV data. *Remote Sensing of Environment*, 40(2), 137–51.
- Green, A., Berman, M., Switzer, P., & Craig, M. (1988). A transformation for ordering multispectral data in terms of image quality with implications for noise removal. *IEEE Transactions on Geoscience and Remote Sensing*, 26(1) (Jan), 65–74.
- Green, R., Eastwood, M., Sarture, C., Chrien, T., Aronsson, M., Chippendale, B., et al. (1998). Imaging spectroscopy and the airborne visible infrared imaging spectrometer (AVIRIS). *Remote Sensing of Environment*, 65(3), 227–48.
- Green, R. (2007). AVIRIS and related 21st century imaging spectrometers for earth and space science, in *High Performance Computing in Remote Sensing*, Chapman and Hall/CRC Press, 335–58.
- Hald, A. (1999). On the history of maximum likelihood in relation to inverse probability and least squares. *Statistical Science*, 14(2) (May), 214–22.
- Haralick, R., Shanmugam, K., & Dinstein, I. (1973). Textural features for image classification. *IEEE Transactions on Systems Man and Cybernetics*, SMC3(6) (Nov), 610–21.
- Harsanyi, J., & Chang, C. (1994). Hyperspectral image classification and dimensionality reduction - an orthogonal subspace projection approach. *IEEE Transactions on Geoscience and Remote Sensing*, 32(4) (Jul), 779–85.

- He, D., & Wang, L. (1990). Texture unit, texture spectrum, and texture analysis. *IEEE Transactions on Geoscience and Remote Sensing*, 28(4) (Jul), 509–12.
- Healey, G., & Slater, D. (1999). Models and methods for automated material identification in hyperspectral imagery acquired under unknown illumination and atmospheric conditions. *IEEE Transactions on Geoscience and Remote Sensing*, 37(6) (Nov), 2706–17.
- Humphrey, M. (2003). *Texture Analysis of High Resolution Panchromatic Imagery for Terrain Classification*. Master's Thesis, Naval Postgraduate School, Monterey, CA. June
- Jensen, J., Hodgson, M., Christensen, E., Mackey, H., Tinney, L., & Sharitz, R. (1986). Remote-sensing inland wetlands - a multispectral approach. *Photogrammetric Engineering and Remote Sensing*, 52(1) (Jan), 87–100.
- Kruse, F., Lefkoff, A., Boardman, J., Heidebrecht, K., Shapiro, A., Barloon, P., et al. (1993). The spectral image-processing system (SIPS) - interactive visualization and analysis of imaging spectrometer data. *Remote Sensing of Environment*, 44(2–3), 145–63.
- Kruse, F., Boardman, J., & Huntington, J. (2003). Comparison of airborne hyperspectral data and EO-1 Hyperion for mineral mapping. *IEEE Transactions on Geoscience and Remote Sensing*, 41(6) (Jun), 1388–400.
- Lennon, M., Mouchot, M., Mercier, G., & Hubert-Moy, L. (2000). *Segmentation of hedges on CASI hyperspectral images by data fusion from texture, spectral and shape analysis*. IGARSS IEEE 2000 Proceedings, Vol 2, 825–7.
- Levine, M. (1969). Feature extraction - A survey. *Proceedings of the IEEE*, 57(8) (Aug), 1391–407.
- Li, J., & Narayanan, R. (2004). Integrated spectral and spatial information mining in remote sensing imagery. *IEEE Transactions on Geoscience and Remote Sensing*. 42(3) (Mar), 673–85.
- Mianji, F., Zhang, Y., Gu, Y., & Babakhani, A. (2009). *Spatial-spectral data fusion for resolution enhancement of hyperspectral imagery*. IGARSS IEEE 2009 Proceedings, Vol 3, 1011–4.
- Mirzaoff, A., Vogler, S., & Coss, J. (2002). *Kodak multi-sensor IMINT fusion data collection*. International Society of Information Fusion, 792–7.
- Niemann, K., Goodenough, D., Marceau, D., & Hay, G. (1998). *A practical alternative for fusion of hyperspectral data with high resolution imagery*. IGARSS IEEE 1998 Proceedings, Vol 1, 174–6.
- Ohanian, P., & Dubes, R. (1992). Performance evaluation for 4 classes of textural features. *Pattern Recognition*, 25(8), 819–33.

- Olsen, R., Garner, J., & Van Dyke, E. (2003). Terrain classification in urban wetlands with high-spatial resolution multi-spectral imagery. *Sensors, Systems and Next-Generation Satellites VI*, 4881, 686–91.
- Pande, H., Tiwari, P., & Dobhal, S. (2009). Analyzing hyper-spectral and multi-spectral data fusion in spectral domain. *Journal of the Indian Society of Remote Sensing*, 37(3) (Sep), 395–408.
- Pearlman, J., Barry, P., Segal, C., Shepanski, J., Beiso, D., & Carman, S. (2003). Hyperion, a space-based imaging spectrometer. *IEEE Transactions on Geoscience and Remote Sensing*. 41(6) (Jun), 1160–73.
- Randen, T., & Husoy, J. (1999). Filtering for texture classification: A comparative study. *IEEE Transactions on Pattern Analysis and Machine Intelligence*, 21(4) (Apr), 291–310.
- Richards, J., & Jia, X. (2008). Using suitable neighbors to augment the training set in hyperspectral maximum likelihood classification. *IEEE Geoscience and Remote Sensing Letters*, 5(4) (Oct), 774–7.
- Roger, R. (1996). Sparse inverse covariance matrices and efficient maximum likelihood classification of hyperspectral data. *International Journal of Remote Sensing*, 17(3), 589–613.
- Rogge, D., Rivard, B., Zhang, J., Sanchez, A., Harris, J., & Feng, J. (2007). Integration of spatial-spectral information for the improved extraction of endmembers. *Remote Sensing of Environment*, 110(3), 287–303.
- Ryherd, S., & Woodcock, C. (1996). Combining spectral and texture data in the segmentation of remotely sensed images. *Photogrammetric Engineering and Remote Sensing*, 62(2) (Feb), 181–94.
- Sebestyen, G. (1962). Pattern-recognition by an adaptive process of sample set construction. *Ire Transactions on Information Theory*, 8(5), S82-S91.
- Segl, K., Roessner, S., Heiden, U., & Kaufmann, H. (2003). Fusion of spectral and shape features for identification of urban surface cover types using reflective and thermal hyperspectral data. *ISPRS Journal of Photogrammetry and Remote Sensing*, 58(1–2), 99–112.
- Shannon, C. (1997). The mathematical theory of communication. 1963. *M.D. Computing : Computers in Medical Practice*, 14(4), 306–17.
- Strahler, A. (1980). The use of prior probabilities in maximum-likelihood classification of remotely sensed data. *Remote Sensing of Environment*, 10(2), 135–63.
- Sutton, R., & Hall, E. (1972). Texture measures for automatic classification of pulmonary-disease. *IEEE Transactions on Computers*, C 21(7) (Jul), 667–76.
- Vane, G., & Goetz, A. (1988). Terrestrial imaging spectroscopy. *Remote Sensing of Environment*, 24(1), 1–29.

- Waske, B., & Benediktsson, J. (2007). Fusion of support vector machines for classification of multisensor data. *IEEE Transactions on Geoscience and Remote Sensing*, 45(12) (Dec), 3858–66.
- Wilson, T., Rogers, S., & Kabrisky, M. (1997). Perceptual-based image fusion for hyperspectral data. *IEEE Transactions on Geoscience and Remote Sensing*, 35(4) (Jul), 1007–17.
- Zhang, Y. (2001). Texture-integrated classification of urban treed areas in high-resolution color-infrared imagery. *Photogrammetric Engineering and Remote Sensing*, 67(12) (Dec), 1359–65.

THIS PAGE INTENTIONALLY LEFT BLANK

INITIAL DISTRIBUTION LIST

1. Defense Technical Information Center
Ft. Belvoir, VA
2. Dudley Knox Library
Naval Postgraduate School
Monterey, CA
3. Fred A. Kruse
Naval Postgraduate School
Monterey, CA
4. Richard C. Olsen
Naval Postgraduate School
Monterey, CA
5. Dan C. Boger
Naval Postgraduate School
Monterey, CA